AGU PUBLICATIONS

Reviews of Geophysics

REVIEW ARTICLE
10.1002/2014RG000449

Key Points:
- Reviews our understanding of the Earths albedo and factors that shape it
- The albedo of Earth is highly regulated mostly by clouds
- The regulation has surprising consequences, and the implications are discussed

Correspondence to:
G. L. Stephens,
graeme.stephens@jpl.nasa.gov

Citation:
Stephens, G. L., D. O'Brien, P. J. Webster, P. Pilewski, S. Kato, and J.-l. Li (2015), The albedo of Earth, *Rev. Geophys.*, *53*, doi:10.1002/2014RG000449.

Received 28 JAN 2014
Accepted 15 JAN 2015
Accepted article online 26 JAN 2015

The albedo of Earth

Graeme L. Stephens[1,2,3], Denis O'Brien[4], Peter J. Webster[5], Peter Pilewski[6,7], Seiji Kato[8], and Jui-lin Li[1]

[1]Jet Propulsion laboratory, California Institute of Technology, Pasadena, California, USA, [2]Department of Meteorology, University of Reading, Reading, UK, [3]The Meteorological Office, Exeter, UK, [4]OBrien R&D LLC, Livermore, Colorado, USA, [5]School of Earth and Atmospheric Sciences, Georgia Institute of Technology, Atlanta, Georgia, USA, [6]Department of Atmospheric and Oceanic Sciences, University of Colorado Boulder, Boulder, Colorado, USA, [7]Laboratory for Atmospheric and Space Physics, University of Colorado Boulder, Boulder, Colorado, USA, [8]NASA Langley Research Center, Hampton, Virginia, USA

Abstract The fraction of the incoming solar energy scattered by Earth back to space is referred to as the planetary albedo. This reflected energy is a fundamental component of the Earth's energy balance, and the processes that govern its magnitude, distribution, and variability shape Earth's climate and climate change. We review our understanding of Earth's albedo as it has progressed to the current time and provide a global perspective of our understanding of the processes that define it. Joint analyses of surface solar flux data that are a complicated mix of measurements and model calculations with top-of-atmosphere (TOA) flux measurements from current orbiting satellites yield a number of surprising results including (i) the Northern and Southern Hemispheres (NH, SH) reflect the same amount of sunlight within ~ 0.2 W m^{-2}. This symmetry is achieved by increased reflection from SH clouds offsetting precisely the greater reflection from the NH land masses. (ii) The albedo of Earth appears to be highly buffered on hemispheric and global scales as highlighted by both the hemispheric symmetry and a remarkably small interannual variability of reflected solar flux (~0.2% of the annual mean flux). We show how clouds provide the necessary degrees of freedom to modulate the Earth's albedo setting the hemispheric symmetry. We also show that current climate models lack this same degree of hemispheric symmetry and regulation by clouds. The relevance of this hemispheric symmetry to the heat transport across the equator is discussed.

1. Introduction

The incoming energy from the Sun fuels the dynamical, chemical, and biological processes of the Earth system. This energy undergoes quasi-cyclic variations associated with solar activity [*Sofia and Li*, 2001], and speculation about the importance of this variation to climate variability has been a topic of much debate over centuries (*Herschel* [1801], *Koppen* [1873], *Labitzke and van Loon* [1992], *Haigh* [1996], and *Gray et al.* [2010] among many others). The fraction of the incoming solar energy scattered by Earth back to space, about 29% (or 0.29 in fractional units), is referred to as the planetary albedo, and less is generally known about its variation over time. We know that Earth's climate has been relatively stable since the Holocene, with global mean surface temperature varying by about 1 K [*Intergovernmental Panel on Climate Change*, 2001; *Moberg et al.*, 2005]. Because it is reasonable to propose that the Earth's equilibrium temperature has changed by a similar amount, we can reasonably surmise that past variations in albedo have been small. In the absence of climate feedbacks and for the present-day value of 0.29, a 5% change in the magnitude of this albedo corresponds to a global surface temperature change of approximately 1 K [*North et al.*, 1981].

There are many reasons why it is important to understand the variability of the Earth's albedo and the factors that define it:

1. Simple energy balance models of the climate system are unstable to small changes in the amount of energy reflected to space. In these simple models with an albedo overly sensitive to surface temperature, relatively small changes in the absorbed solar energy (the difference between the incoming energy and the outward reflected energy) can swing these models from a near ice-free Earth to a fully ice covered state [*Budyko*, 1969; *Cahalan and North*, 1979].
2. It is also speculated that albedo changes potentially regulate the climate system. Lovelock's Gaia hypothesis [*Lovelock*, 1967], exemplified in the study of "Daisyworld" by *Watson and Lovelock* [1983], suggests that regulation of the system albedo by the adaptation of biota of differing albedos to climate change might in fact buffer the system from the instabilities inherent to earlier energy balance models.

©2015. American Geophysical Union. All Rights Reserved.

3. The reflection of sunlight by clouds provides an important climate change feedback mechanism. Reductions in reflected sunlight related to reduced low cloud amount in global warming simulations [*Clement et al*., 2009] produce a positive feedback, while increases in cloud water content with warming is a form of negative feedback [*Paltridge*, 1980; *Sommerville and Remer*, 1984]. Our inability to quantify these feedbacks with any certainty is recognized as one of the major obstacles in climate change predictions [*Bony and Dufresne*, 2005; *Andrews et al*., 2012; *Vial et al*., 2013].
4. More locally, the Earths albedo appears to be resilient to other internal changes that might otherwise alter the system albedo. Perturbations to the albedo through effects of aerosol on clouds appears to be buffered by compensating processes [*Stevens and Feingold*, 2009] that restrict local albedo changes to changing aerosol influences [*Christensen and Stephens*, 2011; *Chen et al*., 2012]. The implications of these more local compensations to concepts proposed to mitigate climate change through geoengineering cloud albedo [e.g., *Latham*, 2002] are thus profound.
5. Regulation of the Earth's albedo is also central to other important climate feedbacks, including the snow/ice surface albedo feedback as well as cloud feedbacks. *Hall and Qu* [2006], for instance, suggested that the magnitude of the snow-albedo feedback in climate change correlates to present-day seasonal changes of high-latitude surface albedo associated with the seasonal migration of the high-latitude snow line. This is one of several emergent model properties that have been proposed as constraining Earth's equilibrium climate sensitivity [*Caldwell et al*., 2014].
6. It has also been conjectured that the characteristics of the total energy transport from low to high latitudes are insensitive to the structure and dynamics of the atmosphere-ocean system and are determined primarily by external controls such as the solar constant, the size of the Earth, the tilt of the Earth's axis, and the hemispheric mean albedo [*Stone*, 1978; *Enterton and Marshall*, 2010]. The results of *Donohoe and Battisti* [2012] are further consistent with this notion. They show that the maximum in annual mean meridional heat transport differs by approximately 20% among coupled climate models due to model differences in equator to pole planetary albedo.

A review of our understanding of the albedo of Earth seems timely given its importance to climate and given recent progress in the measurement of it. This paper first reviews our understanding of the Earth's albedo as it has progressed to the current time and provides a global perspective of our understanding of the processes that shape it. The scope of discussion of this review centers on the behavior of albedo on monthly to seasonal to interannual timescales afforded by current available global top-of-atmosphere (TOA) satellite data. The perspective of this review is also aided by the use of a simple diagnostic model of Earth's albedo introduced in section 3. The model provides a way of incorporating our most up-to-date global data to isolate surface contributions from atmospheric contributions. When applied to TOA flux data collected from currently orbiting satellites together with matched surface flux data inferred from these and other satellite observations, a number of surprising features about the planet's albedo are revealed as introduced in sections 4 and 5 and discussed further in section 7.

1. We show, as in other studies [*Vonder Haar and Suomi*, 1971; *Voigt et al*., 2013], that the Northern and Southern Hemispheres (NH and SH) reflect the same amount of sunlight within 0.2 W m^{-2}. We show clearly how this is achieved as a consequence of reflection from increased amounts of SH clouds offsetting precisely the increased reflection from the larger NH land masses as conjectured by *Vonder Haar and Suomi* [1971]. The spectral distribution of this reflected energy exhibits clear differences between the hemispheres that reinforce our understanding of how the hemispheric symmetry is established.
2. The albedo appears to be highly constrained on the hemispheric and global scale and over interannual timescales. The hemispheric symmetry is an example of such a constraint, and the interannual variability of reflected energy is another example. The interannual variability is small, mostly regulated by the changes to clouds associated with the main modes of climate variability. Overall, these changes occur in a way that minimizes the global effects of clouds on the albedo, buffering the Earth system from large changes.

We also show that the ability of present-day models of climate in simulating the statistical properties of the energy reflected from Earth varies depending upon the metric used. Models produce a much more variable reflected sunlight than observed and fail to reproduce the same degree of hemispheric symmetry. Simple arguments suggest that a symmetric energy balance implies zero net cross equatorial transport of heat that is also a condition of a steady state. Although Earth is very near this symmetric state, it is out of energy balance, with less outgoing longwave radiative (OLR) emitted from the SH than the NH. This hemispheric

©2015. American Geophysical Union. All Rights Reserved.

asymmetry in OLR contributes to the approximate 0.6 W m^{-2} imbalance observed and is associated with offsetting transports of heat from north to south in the atmosphere and from south to north in the oceans.

2. Historical Review

The TOA albedo is one of the main components of the Earth's energy budget and thus our understanding of it follows the evolution of our understanding of the energy balance of Earth. The relatively long history of studies of the Earth's radiation balance can be thought of as occurring in two main eras delineated by the beginning of the space age with the launch of Earth-orbiting satellites. Excellent reviews of the history of the Earth's Radiation Budget (ERB) are given by *Hunt et al*. [1986] for the presatellite era and by *House et al*. [1986] for the satellite era before the Earth Radiation Budget Experiment (ERBE) [*Barkstrom*, 1984] and by *Kandel and Viollier* [2005, 2010] for the post-ERBE era. Our current understanding of solar irradiance variability and the measurement of it has also been reviewed in a number of publications [e.g., *Myre et al*., 2013], and both *Stephens et al*. [2012] and *Stevens and Schwartz* [2012] provide a broader review of Earth's energy balance including the ERB.

2.1. The Presatellite Era

As *Hunt et al*. [1986] note, presatellite-era estimates of the Earth's albedo changed considerably over time. Perhaps, the earliest presatellite estimates of albedo are found in the work of *Abbot and Fowle* [1908] who deduced the global albedo by combining calculations of the solar transfer through three different columns: the cloud-free column (assumed to be 48% of the Earth's surface), a column with cloud below 1800 m (20.8%), and a column with cloud above 1800 m (31.2%). Their value of 0.37 was close to the value of 0.325 of *London* [1957] which was one of the last of the presatellite estimates. Abbott and Fowle were forced to introduce various assumptions about the albedo of clouds at different levels, the values of surface albedo, and the ratio of diffuse to direct radiation in the clear skies. This estimate was soon to be revised upward by *Dines* [1917] to 0.50 based on radiative equilibrium constructs and then decreased by *Aldrich* [1922] to 0.43 on the basis of a balloon measurement. In both cases, the albedo of cloud was significantly larger than measured today, with Aldrich assuming 0.78 taken from observations of fog layers below Mount Wilson.

In a series of papers, *Simpson* [1928a, 1928b, 1929] advanced the topic of radiation budget and provided geographical distributions of all components of the budget. Although Simpson adopted *Aldrich*'s [1922] planetary albedo of 0.43, he was the first to recognize the importance of the spectral distribution of water vapor absorption and calculated the distribution of incoming and outgoing radiation as a function of latitude and season, making use of the cloud distributions produced by *Brooks* [1930]. Simpson came to the conclusion that the Earth was in radiative balance to within an accuracy of 2%. However, the high albedo (0.43) assumed resulted in too low value for the solar energy absorbed by the Earth and its atmosphere and consequently too low value of the outgoing terrestrial radiation.

Bauer and Phillips [1934, 1935] improved upon the results obtained by Simpson using a scheme that involved the variation of albedo with latitude, although these albedos relied heavily on the previously assumed cloud albedo of 0.78 derived by *Aldrich* [1922]. More advanced estimates of *Fritz* [1948, 1950] and *Robinson* [1956, 1958] converged on a value of approximately 0.35. *Houghton* [1954] also estimated the planetary albedo to be 0.34 with a minimum of 0.28 in the subtropics and a maximum of 0.67 at the poles. London's subsequent estimate was widely considered to be the most definitive estimate of albedo prior to the emergence of satellite observations.

Over this same period of time, a number of competing estimates of Earth's albedo were provided by the astronomical community. These were based on observations of the earth-lit Moon that are now referred to as earthshine observations. These earthshine observations in effect integrate the brightness of large areas of the Earth. One of the earliest of these estimates was that of *Very* [1912], who measured the relative brightness of the sunlit and earth-lit portions of the lunar disk and that of the neighboring sky. He deduced that the Earth's albedo must be more than 5 times that of the Moon. Because he used an unreasonably high value (0.174) for the Moon's albedo, he obtained the value of 0.89 for the Earth, which then implied an unrealistically high value of the solar constant. *Russell*'s [1916] reanalysis of Very's data leads to values of the Earth's albedo in the range 0.41–0.49.

©2015. American Geophysical Union. All Rights Reserved.

Table 1. Summary of Milestone Studies of the Earth's Albedo That Highlight the Steps in the Evolution Toward Today's Estimate

Investigation	Albedo	Comments
Abbot and Fowle [1908]	0.37	Forced to make gross assumptions about cloudiness
Dines [1917]	0.50	Influenced by balloon measurements
Aldrich [1922]	0.43	Cloud albedo of 0.78 inferred from measurements of fog below Mount Wilson
Simpson [1929]	0.43	Adopted from Aldrich, recognized importance of water vapor and variations with latitude
Fritz [1950] and *Robinson* [1958]	0.35	Refined variation with latitude
Houghton [1954]	0.34	Minimum value of 0.28 in subtropics, 0.67 polar
London [1957]	0.32	Offered a refined zonal structure
Very [1912] and *Danjon* [1928, 1936]	0.89; 0.39, 0.29	Extrapolated earthshine measurements
Vonder Haar and Suomi [1971]	0.30	First estimate from research satellite measurements
ERBE, CERES, 1984–up to present	0.29	From dedicated Earth radiation budget observing systems

Danjon [1928, 1936] also used earthshine observations to determine the albedo of Earth. From the brightness ratio of the sunlit and earth-lit regions of the Moon and the variation with phase of the brightness of the Moon, *Danjon* [1936] computed an albedo of 0.39 correcting his earlier estimate of 0.29 [*Danjon*, 1928] that was closer to today's postsatellite era values included in Table 1. Ironically, he rejected this lower value in his 1936 publication arguing the lunar brightness phase variation law on which it was based to be in error. Danjon also found substantial seasonal variations of the albedo, from 0.30 in August to 0.50 in October that coincidently appear in more modern earthshine estimates but are not observed in satellite Earth radiation budget records (next section).

Pallé et al. [2004] claimed to have observed significant increases in albedo between 1997 and 2005 from more recent earthshine measurements. These inferred albedo trends were at variance with global satellite observations based on the broadband CERES (Clouds and the Earth's Radiant Energy System) [*Wielicki et al*., 2005] as highlighted in Figure 1. It was later shown through simulated earthshine observations both at the top of atmosphere and surface that the differences shown in Figure 1 in part could be explained by the corrections applied to translate the surface earthshine observations to effective TOA observations [*Loeb et al*., 2007]. Incorrect adjustments to the earthshine observations produce a TOA albedo that is much more variable than observed by CERES.

2.2. The Postsatellite Era

Estimates of Earth's albedo have remained largely unchanged from the value of 0.30 deduced from earliest measurement first from the Explorer-7 satellite observations in 1959 [*Kandel and Viollier*, 2010]. This value was later confirmed from the Nimbus satellite measurements by *Vonder Haar and Suomi* [1971] and *Jacobowitz et al*. [1984]. This value is also only slightly different from the current estimate of 0.29 from CERES observations [*Wielicki et al*., 1996] described later. While these satellite-based values have changed little over time, the confidence level of the estimates has greatly increased as both accuracy of instruments and algorithms to derive albedo improved. The accuracy is estimated to be 2% for the ERBE shortwave scanner instruments and 1% for the CERES SW instruments [*Wieliki et al*., 2006; *Loeb et al*., 2009]. The estimated stability of the observed reflected flux by CERES instruments is 0.3 W m^{-2} per decade [*Loeb et al*., 2007].

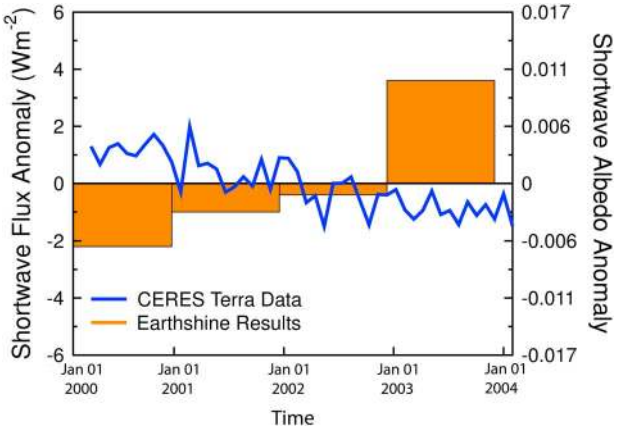

Figure 1. Comparison of global reflected solar flux anomalies for 2000–2003 in blue according to CERES on the NASA Terra spacecraft. A portion of the earthshine record of *Pallé et al*. [2004] is shown in orange (modified from *Wielicki et al*. [2005]).

3. A Simple Model of Reflected Sunlight and Albedo

Simple models of reflected sunlight serve a number of useful purposes. Remote sensing methods based on interpretation of

©2015. American Geophysical Union. All Rights Reserved.

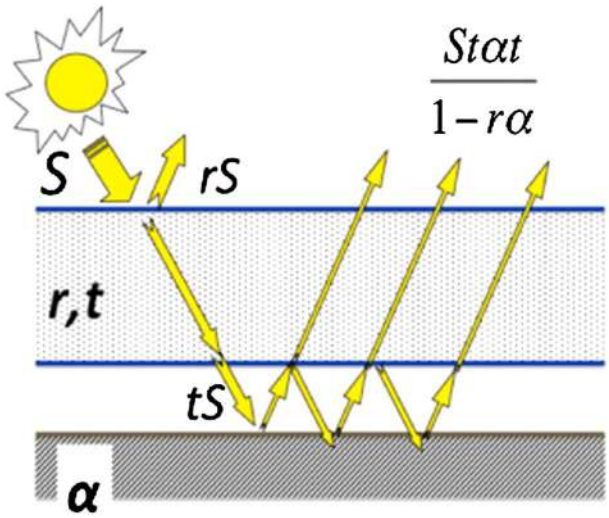

Figure 2. Schematic of a reflecting system composed of a single scattering and absorbing layer of atmosphere over a reflecting surface of albedo α and illuminated by a flux S. The intrinsic scattering properties of the atmosphere are governed by the reflectance r and transmittance t. The total reflectance of the system (system albedo) is given by (6b) and includes the reflected energy from the layer rS plus the multiple scattering between the surface and atmosphere.

sunlight reflected off clouds or aerosol, for example, employ simple models [e.g., *Stephens and Kummerow*, 2007] usually in the form of that illustrated in Figure 2. Similar models have also been invoked to interpret observations of the Earth's radiation budget [*Stephens and Greenwald*, 1991]; and more recently, such low-complexity models have been promoted in climate diagnostic studies to interpret changes in reflected sunlight associated with changes in the climate system [e.g., *Taylor et al*., 2007]. These latter studies seek to understand climate feedbacks such as snow/ice feedbacks, cloud feedbacks, land cover influences, and responses of the biosphere to warming which require a way of separating the changes in surface reflection from changes in atmospheric scattering. The simple model of the Earth's reflected flux and albedo introduced here provides the means to make such distinctions.

The main elements of the model are illustrated in Figure 2. As with most models of this type, it treats the atmosphere as a single absorbing-scattering layer overlying a reflecting surface. For the applications of this study, the fluxes in and out of the top and bottom of the layer are considered known from observations and define the following system quantities:

$$\text{The system reflectance } (=\text{albedo}): R = F^{\uparrow}_{\text{TOA}}/S \tag{1}$$

$$\text{The system transmittance} \quad T = F^{\downarrow}_{S}/S \tag{2}$$

where $S = F^{\downarrow}_{\text{TOA}}$ is the incoming solar flux at the TOA. The system absorption then follows as $A = 1 - R$. The objective is to examine the relation between the system properties A, R, and T and the inherent atmospheric layer reflection and transmission properties r, t, and the surface albedo

$$\alpha = F^{\uparrow}_{S}/F^{\downarrow}_{S} \tag{3}$$

which then provides a way of associating the factors that influence r and t and the separate influence of α on these system properties R, T. The relationships between the fluxes at the boundaries of the atmosphere to the inherent properties of the atmosphere follow from application of the interaction principle [*Flatau and Stephens*, 1988]:

$$F^{\uparrow}_{\text{TOA}} = r_{+}S + t_{+}F^{\uparrow}_{S} \tag{4a}$$

$$F^{\downarrow}_{S} = t_{-}S + r_{-}F^{\uparrow}_{S} \tag{4b}$$

where the quantities $r_{\pm}$ and $t_{\pm}$ are the intrinsic reflection and transmission properties of the atmospheric layer and $1 - r - t$ is the layer absorption which differs from the system absorption A by the amplification effects of reflection and absorption of the surface on the latter. The ± sign refers the polarity (direction) of the flow and typically $r_{+} = r_{-}$ and $t_{+} = t_{-}$ as now assumed with the "+" and "−" subscripts now dropped. The model of *Taylor et al*. [2007] also sets $r_{+} \neq r_{-}$ and has the added unrealistic assumption that absorption occurs only on the incident radiation's first transit (after which the energy in the spectral bands where significant absorption occurs is assumed to be substantially depleted). The combination of (4b) and (3) yields

$$T = \frac{F^{\downarrow}_{S}}{S} = \frac{t}{1 - r\alpha} \tag{5a}$$

$$R = r + \frac{t\alpha t}{1 - r\alpha} \tag{5b}$$

©2015. American Geophysical Union. All Rights Reserved.

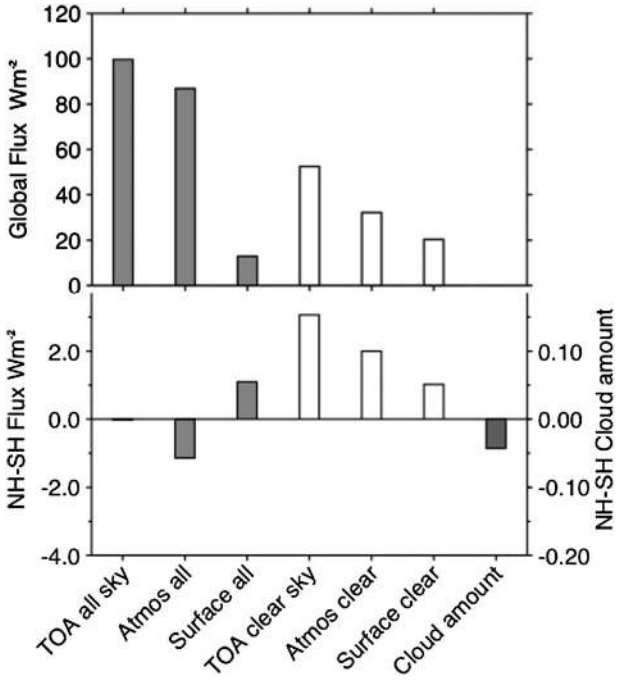

Figure 3. (top) The all-sky and clear-sky global, annual mean reflected fluxes separated into the two main components. (bottom) The difference between hemispheric annual mean all-sky and clear-sky reflected fluxes and the individual components that comprise these fluxes. These hemispheric differences are defined as the NH minus SH, and the all-sky difference is 0.05 W m^{-2}. Also presented for reference is the hemispheric difference in cloud amount (expressed in absolute units) derived from satellite radar and laser data (see text).

According to ((5b)), there are two main contributions to the system albedo—one contribution from atmospheric scattering r and now referred to as the atmospheric contribution and the second term being the surface contribution involving the multiple reflections between the surface and atmosphere. Clouds dominate the atmospheric scattering contribution through a combination of macroscopic properties including cloud amount and intrinsic properties that define the albedo of clouds themselves [*Stephens*, 2005]. The specific influence of these cloud properties has been widely studied, and a review of this literature is considered beyond the scope of this review.

Since the system albedo, R, system transmission, T, and the surface albedo, α, are known from the given boundary fluxes, then ((5a)) and ((5b)) can be inverted to yield

$$t = \frac{[1 - \alpha R]}{1 - \alpha^2 T^2} \tag{6a}$$

$$r = R - t\alpha T \tag{6b}$$

which is the relation between intrinsic properties of the atmosphere (r and t) and the fluxes that exit the layer (SR and ST). The main outputs of the model quantities examined are thus the albedo R (and equivalently the reflected flux SR), the atmospheric contribution to the albedo (r), the surface contribution ($t\alpha t/(1 - r\alpha)$), and the product of these components with S to define the respective flux contributions.

4. Global and Hemispheric Characteristics Inferred From Present-Day Satellite Measurements

We use 13 years of edition 2.7r of Energy Budget Adjusted Fluxes (EBAF) [*Loeb et al*., 2009] and matching surface flux data [*Kato et al*., 2011]. Since these data are matched, they can be applied in (2), (3), (6a), and (6b) to infer the different contributions of the planetary albedo. The algorithms used to derive these fluxes are described in detail elsewhere [e.g., *Wielicki et al*., 1998; *Loeb et al*., 2003, 2005; *Kato and Loeb*, 2005 and *Kato et al*., 2011, 2013] and are not reviewed here. These fluxes are available as monthly means, and the properties of these fluxes are now reviewed. Thus, we do not review the diurnal cycle of albedo and the properties that influence it as the effect of the diurnal cycle on monthly mean fluxes and albedo can be considered to be small. Diurnal cycle effects on trends and variability of albedo over tropics are negligible [*Taylor and Loeb*, 2013], and the global annual mean reflected shortwave irradiance increases by 1% when the diurnal cycle is considered in the estimate [*Doelling et al*., 2013]. The variability of the diurnal cycle of TOA albedo over tropics is discussed by *Taylor* [2014], the effect of diurnal cycle of cloud properties on the albedo has also been investigated by *Hartmann et al*. [1991] and *Haeffelin et al*. [1999].

The global, annually averaged reflected all-sky and clear-sky fluxes, and the surface and atmospheric contributions calculated from (5b) and (4b) are summarized in Figure 3. The hemispheric differences between the TOA flux and the components of this flux are also highlighted in Figure 3 (bottom). Maps of the reflected fluxes and the components of these fluxes appear in Figure 4. Notable results drawn from both figures are the following:

©2015. American Geophysical Union. All Rights Reserved.

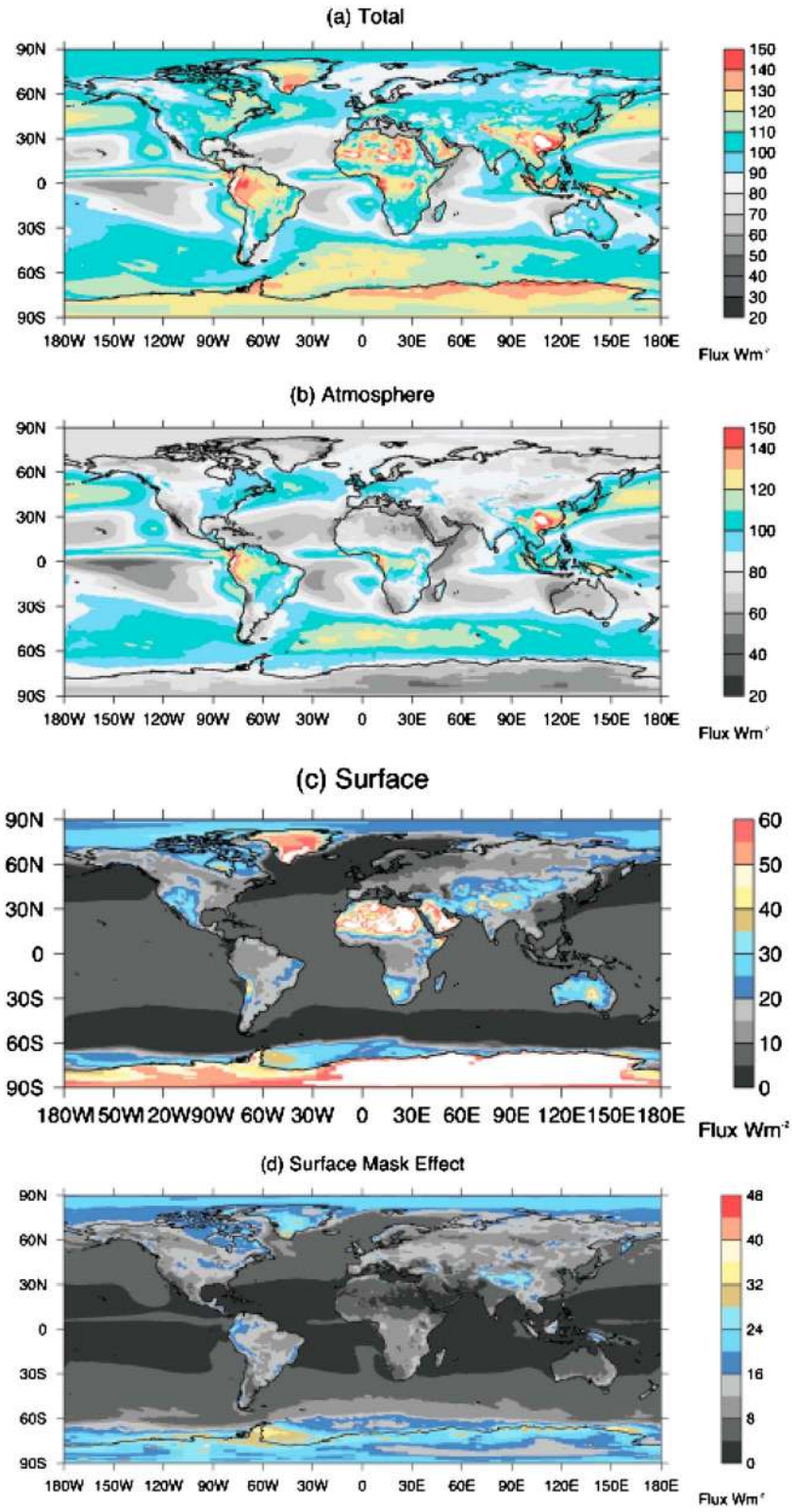

Figure 4. Global distributions of (a) the annual mean all-sky reflected flux, (b) the contribution by atmospheric scattering, and (c) the contribution by the surface reflection where (a) = (b) + (c). (d) The difference between the clear-sky surface contribution and the all-sky surface contribution. This difference represents the amount of clouds mask the actual surface reflection, thus reducing the amount of sunlight reflected from the surface by this amount.

©2015. American Geophysical Union. All Rights Reserved.

1. According to these CERES EBAF data, the global, annual mean all-sky reflected flux is 99.7 W m^{-2} (equivalent to a global albedo of 0.293) and the clear-sky reflected flux is 52.4 W m^{-2} (an albedo of 0.149). The difference between these fluxes (47.3 W m^{-2}) is usually taken to be a measure of the cloud influence on the radiative flux. The atmospheric contribution to the all-sky reflected flux (*rS*) is 86.9 W m^{-2} which is dominated by clouds as evident in the resemblance of the global distribution of this contribution (Figure 4b) to the distribution of clouds [e.g., *Stubenrauch et al*., 2013]. The atmospheric contribution to the clear-sky reflected flux is 32.2 W m^{-2}. The difference between all-sky and clear-sky atmospheric contribution is 54.7 W m^{-2} and is a measure of the actual contribution of scattering by clouds to the reflected flux, whereas the all-sky difference minus clear-sky difference of 47.3 W m^{-2} is a measure of the net effect of clouds on the TOA flux. The reason this scattering contribution is larger than derived from the more common all-sky minus clear-sky difference lies in the differences of the surface contributions. The all-sky surface contribution (12.9 W m^{-2}) is less than the equivalent clear-sky surface contribution (20.4 W m^{-2}) with the 7.5 W m^{-2} difference being shifted to clouds and represents the effects of clouds that overlie reflecting surfaces below that mask the contributions of these surfaces on the TOA flux. That is clouds reflect an extra 7.5 W m^{-2} that would otherwise be reflected by the surface had clouds not be present. This cloud masking effect of the surface has been noted in other studies such as *Soden et al.* [2008] who recognize that surface albedo feedback is overestimated by ~0.3 W m^{-2} K^{-1} when only clear-sky fluxes are used.
2. The lack of flux and albedo difference between hemispheres is remarkable. On the annual average, each hemisphere reflects the same amount of solar energy (less than 0.2 W m^{-2} difference from the data shown in Figure 3 and *Voigt et al*. [2013]) despite the obvious differences in surface albedo between hemispheres. The component analysis reveals this symmetry between hemispheres results from a surprising degree of cancelation between hemispheric differences in the atmospheric and surface all-sky contributions. The surface contribution is larger in the NH as expected, whereas the atmospheric contribution is correspondingly larger in the cloudier SH. The difference in hemispheric cloud amount also shown in Figure 3 is area weighted and given in absolute units. This cloud amount difference is derived from a 4 year average of CloudSat/CALIPSO 2B-GEOPROF-LIDAR cloud occurrence data [*Mace et al*., 2009]. In contrast to the all-sky case, the hemispheric differences of clear-sky fluxes is about 3 W m^{-2} with almost 2 W m^{-2} due to interhemispheric differences in atmospheric scattering and a smaller contribution from surface reflection differences. The atmospheric component difference can be explained mostly by hemispheric differences in aerosol optical depth (AOD). The decadal mean AODs used to produce the CERES surface flux data are, respectively, 0.14 and 0.07 for the NH and SH. Assuming a global ocean aerosol radiative efficiency of 30–40 W m^{-2} (the radiative forcing per unit AOD) [*Loeb and Manalo-Smith,* 2005], then the contribution to the NH clear-sky flux by aerosol is ~4–6 W m^{-2} versus 2–3 W m^{-2} for the SH.
3. Annual mean maps of the reflected flux, and the atmospheric and surface contributions to this flux are provided in Figures 4a–4c, respectively. The atmospheric scattering that is so influential to the observed reflected fluxes in the lower latitudes mirrors the cloudiness of these latitudes. Figure 4d is the flux difference between the clear-sky surface component of the flux and the all-sky surface component and thus provides a map of the cloud masking effect on surface reflection described above. This masking occurs mostly over the land mass areas of the NH and notably the polar regions of both hemispheres. The masking effect can be locally large over the brightest surfaces especially at higher latitudes where clouds effectively reduce the surface contribution by approximately 50%.

5. Time and Space Characteristics Inferred From Present-Day Satellite Measurements

Here we review the time and space variability of the albedo according to global CERES observations. Given the sampling nature of these global observations, the focus of this discussion is on monthly and longer timescales. Prior to the development of the growing CERES record considered here, and because of short lifetime of the ERBE scanner instrument and the more limited coverage of the Earth Radiation Budget Satellite nonscanner instrument, most of our understanding of interannual variability is derived from the Nimbus 6 and 7 instrument record [e.g., *Smith and Smith*, 1987; *Randel and VonderHaar*, 1990]. From these data we have learned that the main source of tropical albedo variability is from cloudiness variability associated with the El Niño–Southern Oscillation (ENSO) phenomena [*Ringer*, 1997; *Smith et al*., 1990].

©2015. American Geophysical Union. All Rights Reserved.

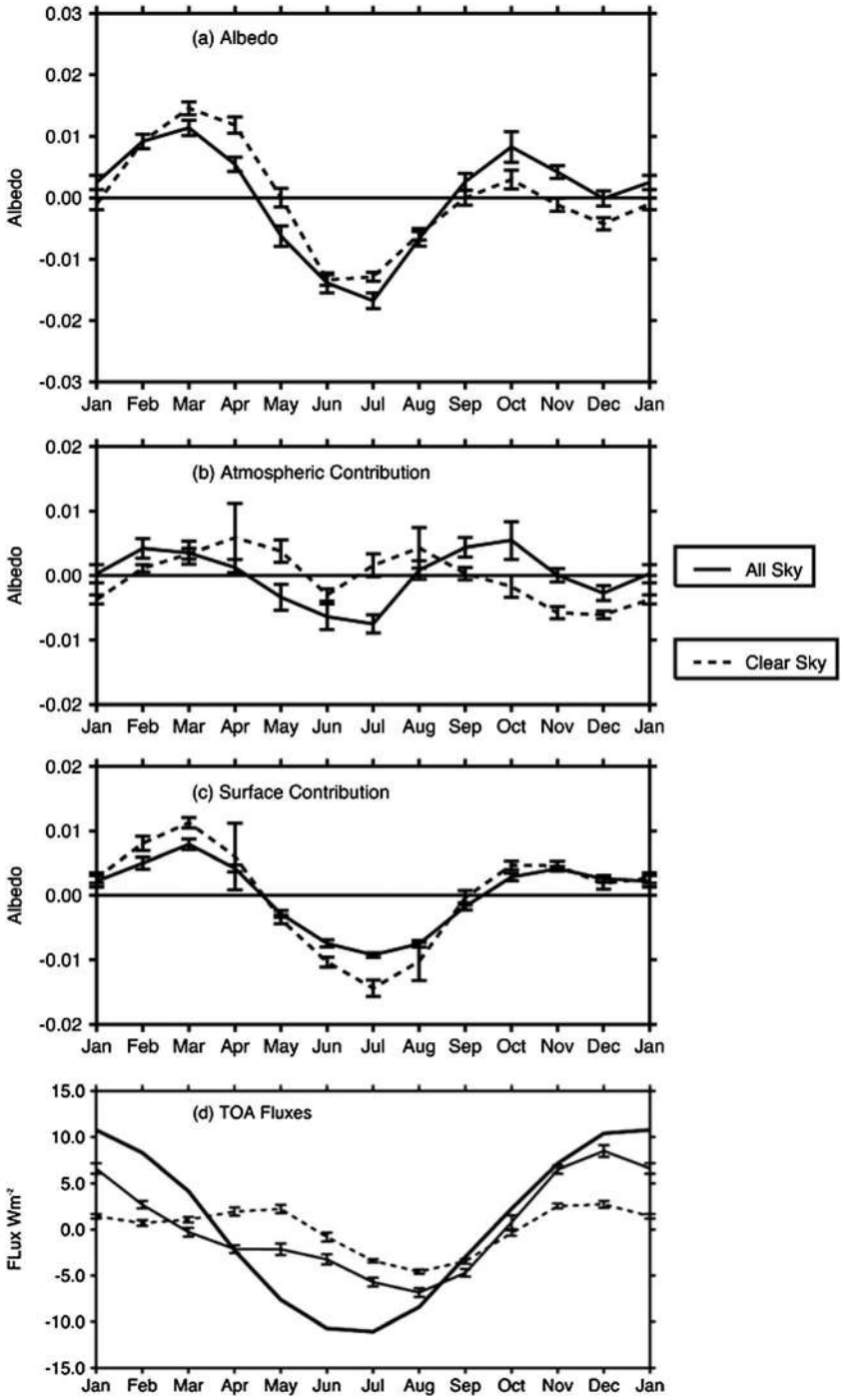

Figure 5. Annual cycles of (a) the globally averaged albedo, (b) the atmospheric, and (c) surface contributions to this cycle. The solid curves are for all-sky fluxes, and the dashed curves are the clear-sky fluxes. The error bars represent the interannual variability. (d–f) The respective cycles of the global mean fluxes where the heavy curve of Figure 5d is the annual cycle of the solar insolation shown for reference. Annual means of all quantities have been subtracted.

Wielicki et al. [2002] and *Wong et al*. [2006] analyzed interannual variability of TOA albedo between 20°S and 20°N using ERBE nonscanner data to find TOA albedo variability over tropics also to be highly correlated with cloud amount [*Loeb et al*., 2007; *Kato*, 2009] and also appears to be influenced by cloud vertical structure [*Cess et al*., 2001; *Allan et al*., 2002]. Interannual variability of TOA albedo from 60°N to 60°S derived from Nimbus-7 ERB instruments and its sensitivity to the cloud amount was investigated by *Ringer and Shine* [1997].

©2015. American Geophysical Union. All Rights Reserved.

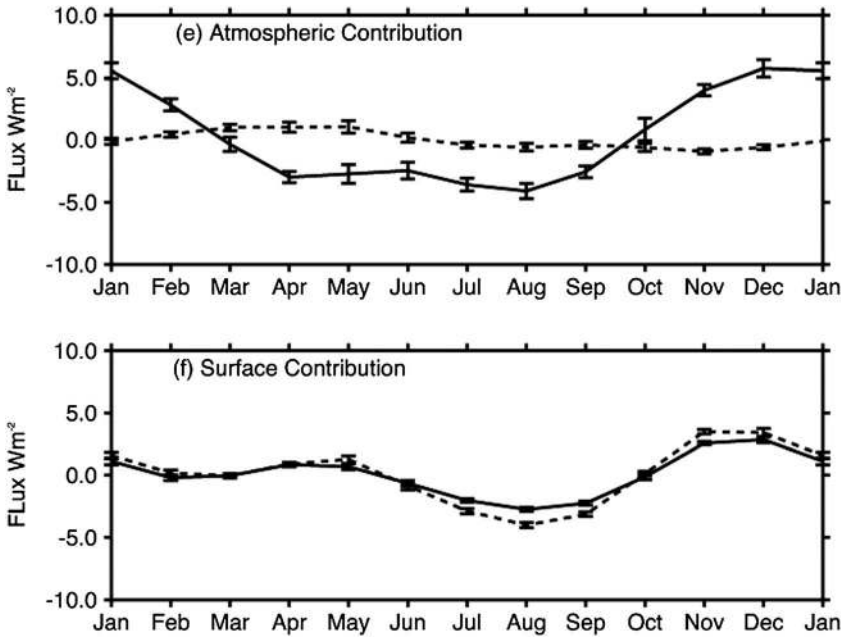

Figure 5. (continued)

A quantitative evaluation of the interannual variability of the global mean albedo is provided by *Kato* [2009], and many of these results are reproduced below.

5.1. The Seasonal Cycle

The seasonal cycle of satellite-derived global mean albedo and global mean reflected fluxes has been discussed in a number of papers. *Stephens et al*. [1981] describe the seasonal cycle contained in the NIMBUS record. *Bender et al.* [2006] examined the seasonal cycle in the ERBE data, and both *Kato* [2009] and *Loeb et al*. [2007] characterize this seasonal cycle from multiple years of CERES. Using radiative transfer simulations of idealized earthshine observations, *Loeb et al*. [2007] further showed how simulated earthshine observations produce a more variable and less coherent seasonal cycle than observed from satellites.

The different satellite-based observations referenced above produce a consistent and repeatable picture of the seasonal cycle shown in Figure 5. The seasonal cycles shown in this figure are an average of 13 annual cycles of CERES EBAF version 2.7r data. What is different about this depiction from earlier studies is the breakdown of the seasonal cycle into its different component parts. Based on the data reviewed, the annual cycle of all-sky albedo has two main maxima (Figure 5a) [also *Stephens et al*., 1981; *Bender et al*., 2006; *Loeb et al*., 2009; *Kato*, 2009]. This seasonal cycle behavior is set in part by the seasonal cycle of surface albedo which has a boreal spring-time maximum resulting from the reflection off the brighter snow-covered land surfaces between 30°N and 60°N (Figure 5c). The second weaker maximum in the boreal fall season is influenced by reflection from midlatitude clouds of the SH (Figure 5b).

The reduced amplitude of the all-sky seasonal cycle compared to clear-sky surface contributions to albedo (solid and dashed curves, respectively, Figure 5c) further illustrates how the presence of clouds globally mask the effects of surface reflection on the TOA fluxes and albedo.

The seasonal cycle of the global mean reflected flux (Figure 5d) approximately follows the annual cycle of the change in global mean solar insolation (amplitude of the latter is 21.8 W m^{-2}, Figure 5d), although the amplitude of the former (13.3 W m^{-2}) does not simply follow as the product of the global mean albedo change and the solar insolation change alone ($0.293 \times 21.8 = 6.4$ W m^{-2}). The difference between 13.3 W m^{-2} and 6.4 W m^{-2} underscores the important influence of large seasonal cycles in the reflected fluxes of the midlatitude and higher latitude. This influence is also evident in the atmospheric contributions shown in Figure 5e and suggested in Figures 4b and 4c.

©2015. American Geophysical Union. All Rights Reserved.

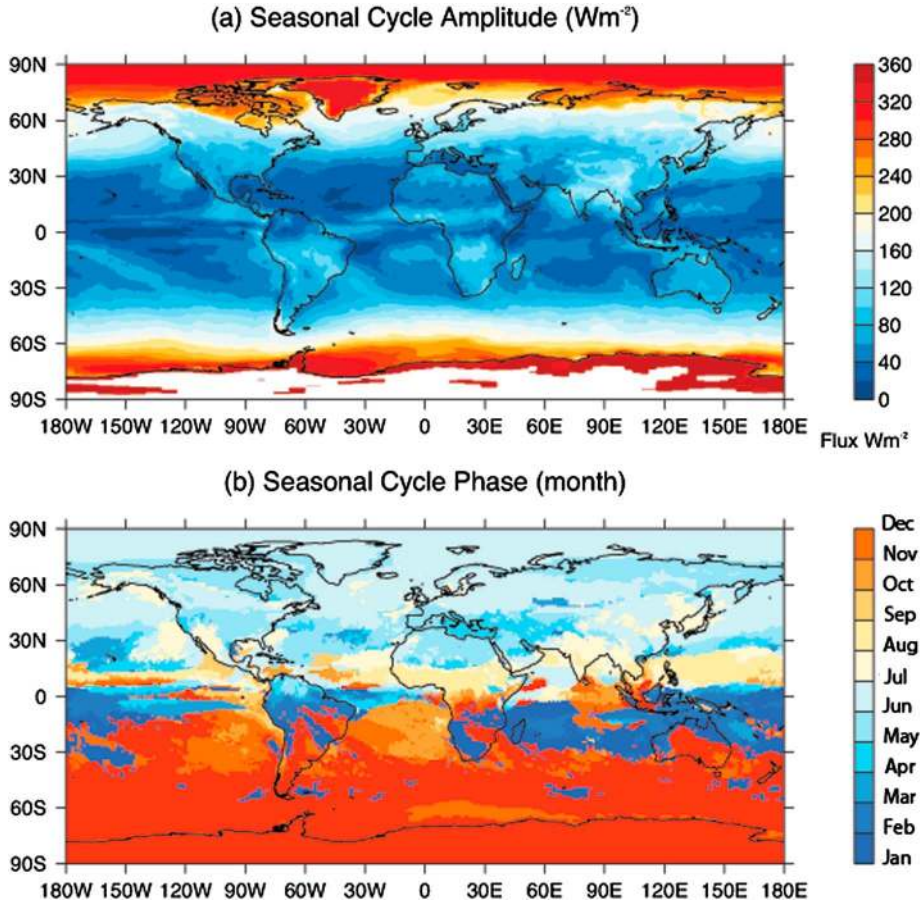

Figure 6. (a) Amplitude and (b) phase of the seasonal cycle of reflected flux. The amplitude is the max-min difference of the annual cycle of reflected flux, and the phase is the month of the maximum flux.

The seasonal cycle of reflected solar flux is shaped by simplifying astronomical factors like Earth-Sun distance and declination angle changes that establish the local solar elevation at any given time and thus the local availability of sunlight. If these factors alone determine both the amplitude and phase of the seasonal cycle of the reflected flux, then the seasonal cycle would have simple and reproducible structures determined merely by the seasonal cycle of incoming solar irradiance. However, the amount of reflected energy and the time at which this reflected energy is maximum are also influenced by local changes to atmospheric and surface properties. These complications are evident in the amplitude (Figure 6a) and phase (Figure 6b) of the seasonal cycle of reflected flux determined from the time and magnitudes of the local maxima and minima of the annual cycle of these fluxes. At lower latitudes, for example, the amplitude defined as the maximum minus the minimum of the local seasonal cycle is strongly influenced by the seasonal cycle of cloudiness. Over land at midlatitude and higher latitude, such as over the continental USA, it is the convolution of the availability of sunlight (maximum in summer seasons) and the brightness of the surface (maximum in early spring) that combine to produce a maximum reflected flux in the spring (Figures 6b and 5f).

5.2. Interannual Variability

There is a remarkable lack of interannual variability in both global albedo and reflected flux. This point has been noted by others such as in *Kato* [2009], and the stability of the albedo extends to the annual zonal means [*Stevens and Schwartz*, 2012] and the hemispherical means [*Voigt et al.*, 2013, 2014]. The variability has been typically quantified as the standard deviation of the deseasonalized monthly reflected flux anomalies. If F is the reflected flux, then the anomalies

$$\Delta F(t,x) = F(t,x) - \overline{F(t,x)} \tag{7}$$

©2015. American Geophysical Union. All Rights Reserved.

Table 2. Annually Averaged Reflected Fluxes Over the Regions Indicated[a]

	Total		Atmosphere		Surface	
Averaging Scale	Flux	$\sigma(x)$	Flux	$\sigma(x)$	Flux	$\sigma(x)$
Global	99.7	0.23	86.9	0.29	12.9	0.10
Tropics (30°N–30°S)	94.3	0.32	82.27	0.37	12.1	0.09
Midlatitude NH(30°–60°N)	103.8	0.52	91.5	0.53	12.3	0.15
Midlatitude SH(30°–60°S)	104.1	0.56	98.9	0.65	5.26	0.10
Polar NH (60°–90°N)	97.0	0.87	78.7	0.87	19.1	0.47
Polar SH (60°–90°N)	118.8	0.68	84.4	1.26	35.5	0.97

[a]The TOA reflected flux ($W\,m^{-2}$) and the contributions to this flux by scattering from the atmosphere and reflection from the surface are given. The standard deviation of the deseasonalized flux as defined by (9) is also given.

are defined with respect to the monthly mean flux computed from 13 values for each month of the year and then area weighted and averaged over a given region x. The standard deviation of fluxes is

$$\sigma_F(x) = \sqrt{\frac{1}{n}\sum_{j=1,n}\left[\Delta F(t_j, x)\right]^2} \tag{8}$$

with $n = 156$ for fluxes averaged over different spatial scales is presented in Table 2. The scales include global averaged fluxes, fluxes averaged between 30°N and 30°S, midlatitude fluxes averaged between 30°N–60°N and 30°S–60°S and polar fluxes (averaged between 60°–90°N and 60°S–90°S). The standard deviation of globally averaged flux is $0.2\,W\,m^{-2}$ which is only 1.4% of the annual cycle and 0.2% of the total global mean reflected flux [e.g., *Kato*, 2009]. This interannual variability systematically increases from the tropics to the midlatitudes to the polar regions. By contrast, the global distribution of the $1° \times 1°$ standard deviation is shown in Figure 7 and has a global mean value of $9.1\,W\,m^{-2}$. The dominant source of this interannual variability arises from the variability in the amount of sunlight scattered by the atmosphere regardless of the scale on which the fluxes are averaged. This source of variability can thus be interpreted as being associated with interannual variability of cloudiness. *Loeb et al*. [2007], for example, show that tropical albedo variations are highly correlated with cloud cover. The analysis of *Smith et al*. [1990] applied to the deseasonalized reflected fluxes also indicates that the cloudiness change associated with ENSO is the main source of interannual variability of reflected flux. The pattern of variability shown in Figure 7, inferred from data of the A-Train [*Stephens et al*., 2002] era, is also consistent with these findings indicating that the regions of highest variability predominantly coincide with those regions where tropical moist convection variability is known to be greatest.

That the interannual variability of TOA flux is primarily determined by the variability of cloudiness is yet further supported by the correlations illustrated in Figure 8. The correlation between the CERES measured TOA June-July-August (JJA) monthly flux anomalies averaged over the eleven JJA seasons and the

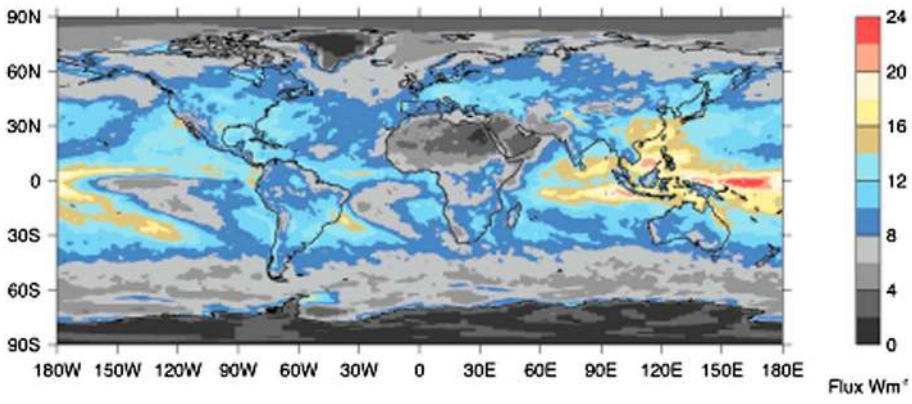

Figure 7. The global distribution of the interannual variability of reflected flux on a $1° \times 1°$ latitude/longitude scale. This variability is expressed by the standard deviation of reflected flux as defined by ((8)).

©2015. American Geophysical Union. All Rights Reserved.

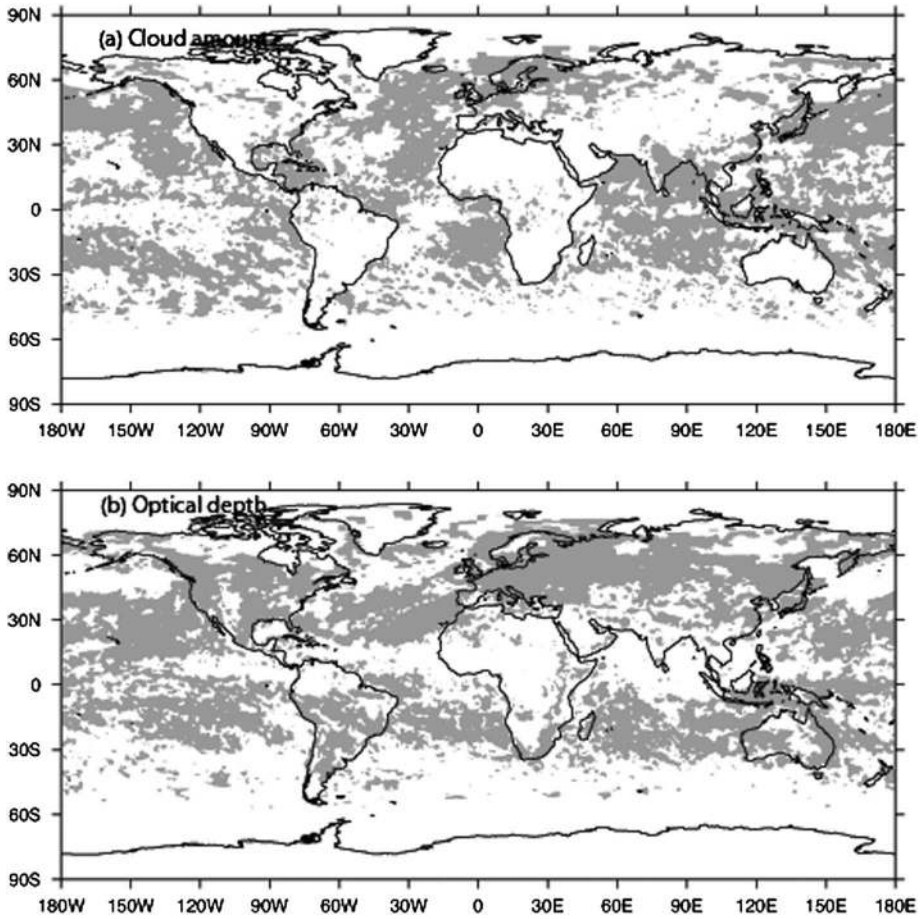

Figure 8. (a) The correlation between the MODIS-based cloud optical depth with the total reflected flux measured by CERES. (b) The correlation between the MODIS-based cloud amount and CERES total reflected flux. Regions where the correlation exceeds 0.8 are shown in grey. Correlations are shown only for the June-July-August season and are based on 13 years of data.

corresponding Moderate Resolution Imaging Spectroradiometer (MODIS) JJA cloud optical depth and cloud amount anomalies are shown in Figures 8a and 8b, respectively. Only the regions of correlations above 0.8 are shaded. The cloud fraction correlations essentially reproduce the results of *Kato* [2009]. Since these maps are for the boreal summer season, the correlations between flux and cloudiness in the higher SH latitudes are low because the incoming solar flux vanishes at these higher latitudes in winter. There are also notable differences between the optical depth and cloud amount correlations. Optical depth correlations over the large land masses tend to be higher than are cloud amount correlations. Correlations between reflected fluxes and cloud optical depths are expected to be more pronounced for thinner clouds since the cloud albedo varies approximately linearly with optical depth than for thick clouds [*Stephens and Tsay*, 1990]. Thus, these results imply that the cloudiness over these land mass regions tends to be optically thinner than over oceans.

5.3. Meridional Heat Transport

The relation between the meridional heat transport and the TOA radiative fluxes is highlighted in Figure 9. Figure 9a is the zonally averaged multiyear average of the CERES EBAF net solar and outgoing longwave radiative (OLR) fluxes, and Figure 9b is the zonal profile of net TOA flux. The latitudes where these fluxes are equal (36.9 ± 0.2° S, 35.0 ± 0.9°N), indicated by the vertical dashed lines, are the latitudes of zero net TOA flux (Figure 9b) and are thus the latitudes of maximum heat transport of each respective hemisphere. The latitude of maximum net TOA flux, which occurs very close to the equator, is also the latitude of zero meridional heat flux. The zonal averaged TOA net flux of Figure 9b highlights the equatorial regions of

©2015. American Geophysical Union. All Rights Reserved.

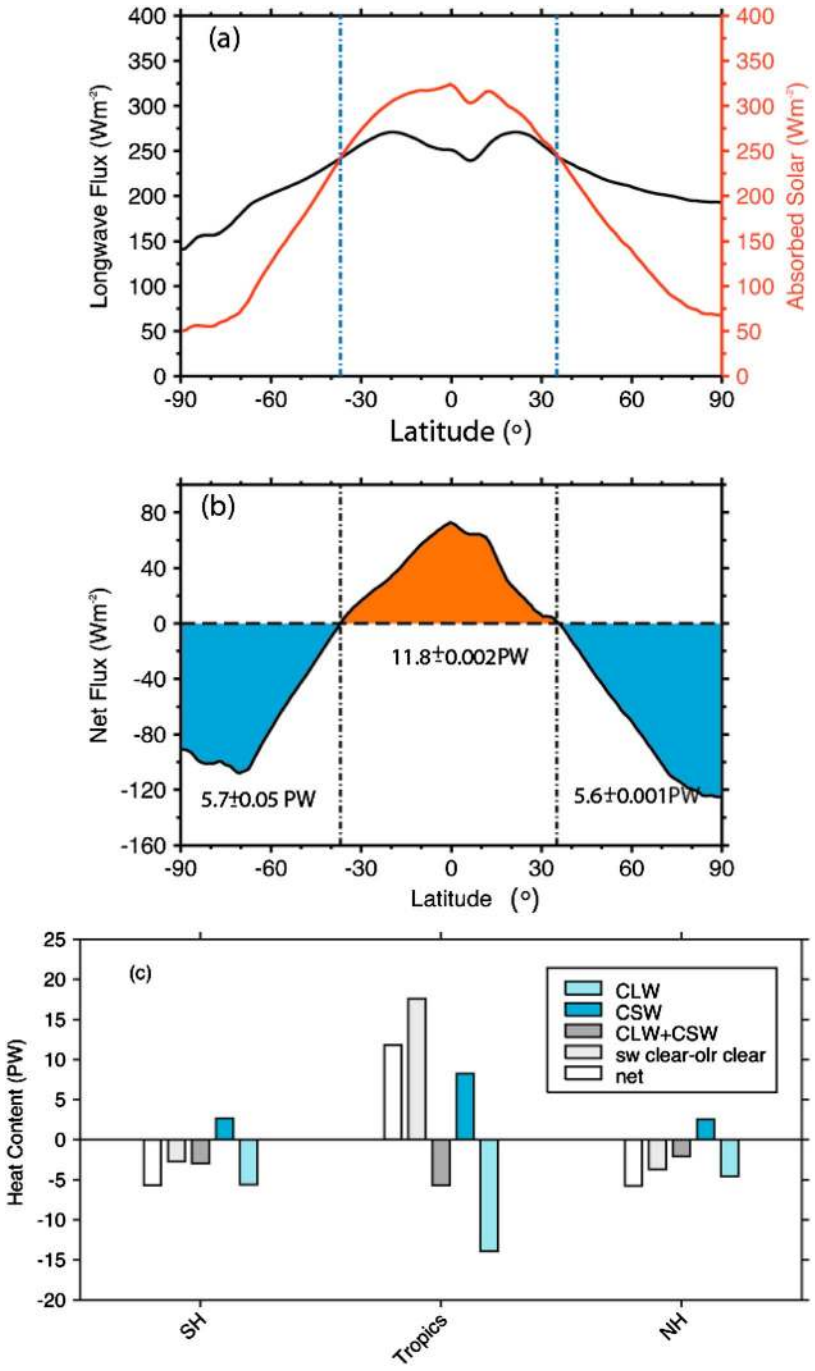

Figure 9. (a) The zonally annually averaged profile of absorbed solar radiation [$S(1-R)$] in red and outgoing longwave radiation (OLR) in black. The fluxes are from CERES EBAF 2.7r and are an average over 13 years. The vertical dashed lines indicate the latitude at which the net TOA flux is zero (i.e., where the absorbed solar flux and OLR are equal). (b) The zonal annual averaged net flux with the integrated heat absorbed for latitudes equatorward of the dashed vertical lines and lost from those latitudes poleward of these lines. These vertical dashed lines are as in Figure 9a and also indicate the latitudes of maximum heat transport. The area integration of the net flux equatorward of these lines (area in red and referred to as "Tropics") corresponds to 11.8 PW, and the area integration of the net flux over latitudes poleward of these lines (referred to as SH and NH "extratropics") corresponds to −5.7 and −5.6 PW for the SH and NH, respectively. (c) The clear and cloudy sky contributions to the heat gained in the tropics and lost in the high-latitude SH and NH extratropics. CLW denoted the cloud longwave radiative effect (the difference of the clear-sky OLR and all-sky OLR). The CSW is the cloud shortwave effect similarly defined as the clear-sky TOA reflected flux minus the all-sky TOA reflected flux. The "sw clear-olr clear" is the difference between the clear-sky TOA absorbed solar minus the clear-sky OLR and "net" is the sum of this difference plus the CLW minus CSW.

©2015. American Geophysical Union. All Rights Reserved.

Table 3. Atmosphere-Ocean Coupled CMIP5 Models Analyzed in This Study

Modeling Center	Acronym	Model Name	Resolution
Canadian Centre for Climate Modeling and Analysis, Canada	CCCMA	CanESM2	2.8125° × 2.7673°, L35
Beijing Climate Center, China	BCC	BCC-CSM1-1	2.8125° × 2.8125°, L26
Commonwealth Scientific and Industrial Research Organization/Queensland Climate Change Centre of Excellence, Australia	CSIRO-QCCCE	mk3.6	1.9° × 1.9°, L18
Geophysical Fluid Dynamics Laboratory, USA	GFDL	cm3	2.5° × 2°, L48
Goddard Institute for Space Studies, USA	GISS	e2-r	2.5° × 2°, L29
Institute for Numerical Mathematics, Russia	INM	cm4	2° × 1.5°, L21
Institut Pierre Simon Laplace, France	IPSL	cm5a	3.75° × 1.8947°, L39
Model for Interdisciplinary Research On Climate/Atmos. Ocean Res. Ins., U. Tokyo/Nat. Ins. Env. Std./Japan Agency for Marine-Earth Sci. and Tech., Japan	MIROC	miroc5	0.5625° × 0.55691°, L56; 1.4° × 1.4°, L40
Model for Interdisciplinary Research On Climate/Atmos. Ocean Res. Ins., U. Tokyo/Nat. Ins. Env. Std./Japan Agency for Marine-Earth Sci. and Tech., Japan	MIROC	miroc-esm	0.56250.55691, L56; 1.4° × 1.4°, L40
Max Planck Institute	MPI	esm-lr	1.875° × 1.875°, L47
Meteorological Research Institute, Japan	MRI	cgcm3	1.125° × 1.1121°, L48
National Center for Atmospheric Research, USA	NCAR	cam5csm1	1.25° × 0.9424°, L30
Norwegian Climate Center (NCC), Norway	NCC	noresm	2.5° × 1.8947°, L26
UK Met Office Hadley Climate Center, UK	MOHC	hadgem2-es	1.875° × 1.25°, L38

positive net flux (in red) and extratropical regions of negative net flux (in blue). The respective amounts of heat gained and lost in these regions calculated from the area-weighted net fluxes are also given, and the error bars quoted are an indicator of the interannual variability of these integrated fluxes. It is also noteworthy that the amounts of heat loss from the extratropics are very close to the same in each hemisphere

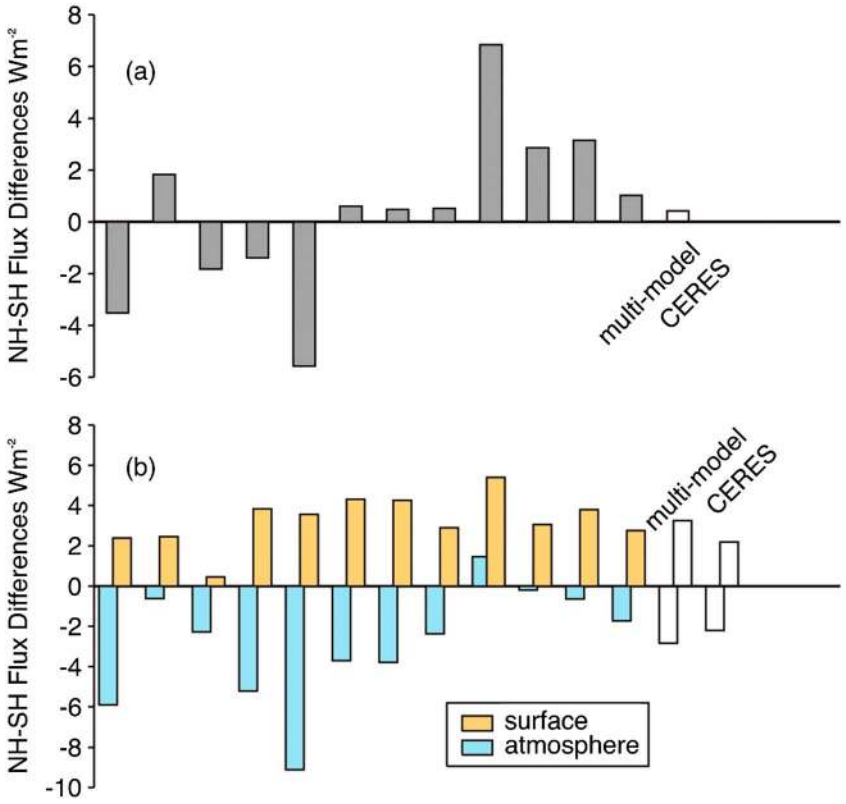

Figure 10. (a) The NH-SH difference in TOA reflected flux from archives of CMIP5 models summarized in Table 3, as well as the mean of all models and the hemispheric difference according to CERES data (see also Figure 3). (b) The SH-NH difference in atmospheric (in yellow) and surface (in blue) contributions to the TOA flux. Monthly data from the last 10 years of the 1% experiment corresponding to the period 1996–2005 are analyzed, whereas the CERES data are for the period March 2000–March 2013.

©2015. American Geophysical Union. All Rights Reserved.

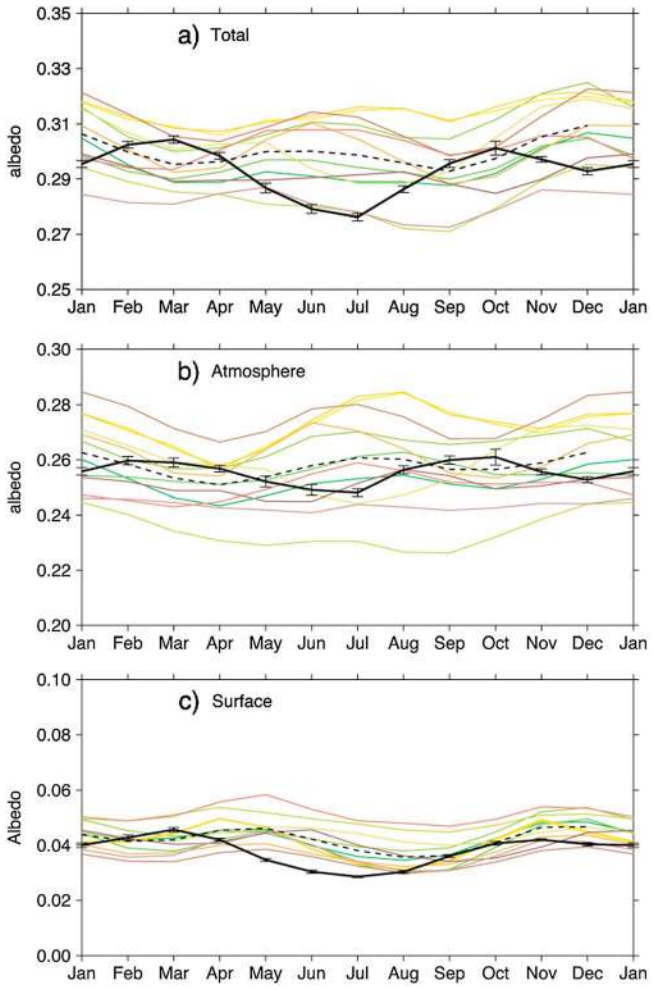

Figure 11. The global mean annual cycle of (a) TOA albedo, (b) atmospheric contribution to the TOA albedo, and (c) the surface contribution to the TOA albedo. The solid lines are CERES observations taken from Figure 5, and the colored lines are 10 year average seasonal cycle of individual CMIP5 models, and the dashed lines are the multimodel mean seasonal cycle.

(5.7 ± 0.05 PW for the SH, 5.6 ± 0.001 PW for the NH), and thus the maximum heat transport by each hemisphere is also approximately the same. This is a consequence of both the albedo and OLR being very close to symmetric about the equator.

Figure 9c illustrates how different components of the radiation balance contribute to the heat accumulated at low latitudes and to that lost at high latitudes. At low latitudes, the heat gain mostly occurs as a result of the excess absorbed solar radiation over the emitted longwave radiation in clear skies. Net cloud effects in the equatorial region are small and negative due to a shortwave cloud effect (CSW) that slightly exceeds the compensating longwave cloud effects (CLW). The heat loss that occurs in the extratropics reveals interesting but expected differences between the hemispheres. For both regions, the longwave emission to space from clear skies exceeds the absorbed solar radiation, making the net effect of clear skies negative but more so in the NH. The net effects of clouds in higher latitudes (CLW + CSW) are also negative and of a similar magnitude to the clear-sky loss. The cloud effects are mostly influenced by the solar radiation reflected by clouds, the latter being larger in the SH thus offering some balance to the increased clear-sky emission of the NH.

6. Performance of Current Day Climate Models

The TOA and surface solar flux data extracted from model-simulated historical climate records are used to diagnose the different components of the TOA flux to compare directly to the flux components of CERES. The model data analyzed here are from the Coupled Model Intercomparison Project Phase 5 (CMIP5) multimodel ensemble archive for the historical experiments in which the known forcings of the twentieth century are applied to the models [*Taylor et al*., 2012]. Monthly data from the last 10 years of this experiment are analyzed for the 13 models identified in Table 3. These data correspond to the period 1996–2005 roughly coinciding with the CERES period. Modeled hemispheric flux differences, the annual cycle of the albedo, the interannual variability, and the meridional heat transport are compared to the observations in Figures 10–12.

From the comparisons presented in these figures, it is evident that models and measurements differ in potentially important ways. Some of these differences have persisted from earlier studies based on CMIP3 archives [e.g., *Bender et al*., 2006].

1. The differences between the hemispheric averaged TOA reflected fluxes and the respective hemispheric differences of the atmospheric and surface contributions are shown in Figures 10a and 10b, respectively. The ensemble model mean and the CERES values are also given for reference. As noted in *Voigt et al.* [2013]

©2015. American Geophysical Union. All Rights Reserved.

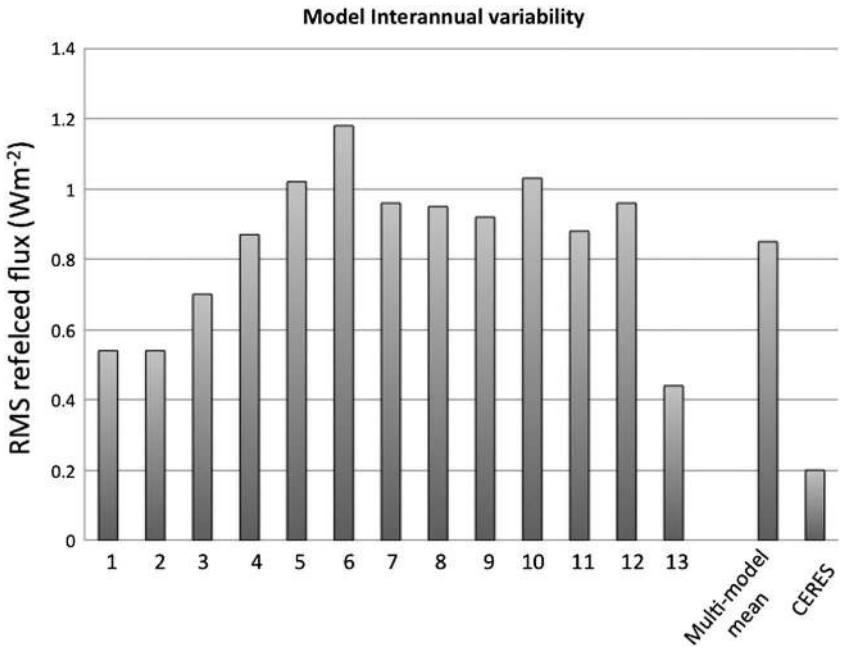

Figure 12. The interannual variability of global mean fluxes of the 13 CMIP5 models compared to the variability of CERES.

and further reproduced in Figure 10a, the observed hemispheric symmetry of reflected flux is not reproduced by models and there is some disagreement between models as to which hemisphere is more reflective. The mean absolute value of the reflected solar flux difference between model hemispheres is 2.4 W m^{-2}, whereas the model ensemble mean is 0.2 W m^{-2}, much closer to that observed. The largest source of disagreement between models lies in the magnitude of the atmospheric contribution. Like the observations, the majority of models produce an atmospheric scattering from the model SH that exceeds the scattering from the NH atmosphere; but unlike the observations, this scattering from model atmospheres does not balance the enhanced reflection from the NH surface. Models also differ in the magnitude of the surface contribution.

2. The global mean seasonal cycle of albedo also varies from that observed, as highlighted by the comparison of the multimodel mean seasonal cycle (dashed curves) to that of CERES (solid curves) in Figures 11a–11c. Even the phase of the seasonal cycle of the surface contribution differs between model and observations. The atmospheric and surface seasonal cycles of albedo offset in the models to produce a multimodel mean seasonal cycle that is much less variable than that observed. According to this comparison, the CMIP5-modeled albedos are consistently higher (by almost 10%) than the CERES values during the boreal summer months (Figure 11a) and this bias has persisted from CMIP3 [*Bender et al*., 2006].
3. There is substantially more year-to-year variability in model reflected flux than observed. The interannual variability of individual models, defined according to (8), varies from slightly more than 2 times to 6 times the interannual variability observed by CERES with the multimodel mean of the interannual variability being 4 times that observed.

7. Discussion

Although the results summarized above are remarkable in a number of ways, they leave a number of unanswered questions about the Earth's albedo.

7.1. Is the Hemispheric Symmetry Purely Coincidental?

Voigt et al. [2013] address this question directly using CERES EBAF data. They produced a large population of nonoverlapping random hemispheric pairs from these data. Each hemisphere covered 50% of Earth's surface area. These hemispheric partitions were then randomly assigned to either one of the two hemispheres, and the difference in reflected flux between these two random hemispheres then calculated.

©2015. American Geophysical Union. All Rights Reserved.

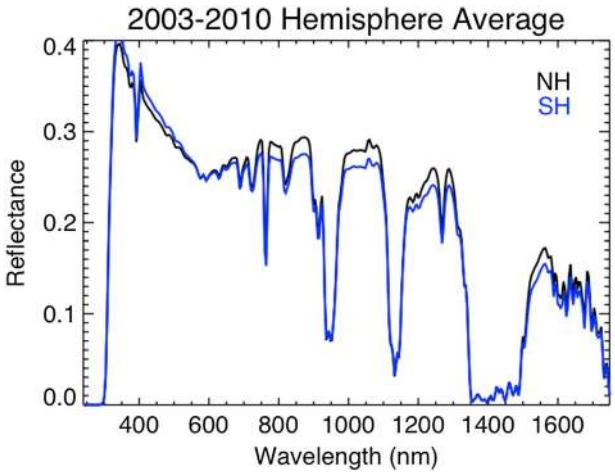

Figure 13. The hemispheric, annual averaged spectral reflectance as measured by SCIAMACHY over the period 2003–2010.

Voigt et al. [2013] find that the number of pairs for which the flux differences are less than or equal to the observed difference occurs in less than 3% of all hemispheric pairs created.

While Voigt et al. could not rule out the possibility of the observed hemispheric symmetry being merely accidental, their results suggest that mechanisms exist to minimize hemispheric differences in reflected shortwave irradiance and planetary albedo in some fundamental way. In a follow up study, *Voigt et al*. [2014] searched for possible mechanisms in simple aqua-planet simulations using a general circulation model coupled to a slab ocean. The experiments were performed with the model initialized with an imposed hemispheric difference in clear-sky albedo. The results showed how the Intertropical Convergence Zone (ITCZ) adapted in such a way as to compensate for the imposed hemispheric asymmetries in clear-sky albedo. The compensation occurred as a shift of the ITCZ and tropical clouds into the darker hemisphere, suggesting that in these model simulations the climate system prefers hemispheric albedo asymmetries to be small and that cloudiness serves as a strong regulator of albedo. *Frierson and Hwang* [2012] argue that cloud biases over the Southern Ocean explain most of the model-to-model differences in the amount of excessive precipitation in SH tropics, suggesting SH cloud biases may be responsible for the double-ITCZ problem in most global climate models. The main point of these studies is they show how adjustments of cloud patterns in one hemisphere can influence the properties of the other hemisphere, thus hinting at possible mechanisms that determine how a symmetric energy balance might be maintained.

7.2. Is the Albedo of Earth Highly Constrained?

1. *Hemispheric Reflectances*. The two model studies referred to above suggest that clouds can adjust through circulation changes to buffer the planet from large changes in albedo. There are many observational threads of evidence that further support the contention that Earth's albedo is highly constrained by changes to cloudiness. The first dramatic, global in scale, example is provided by the property of hemispheric symmetry described above. This symmetry is a result of the effects of increased cloudiness in the SH precisely offsetting the effects of enhanced reflection from the greater NH landmasses (Figure 3). This remarkable result is further reinforced through the interpretation of completely independent measurements of spectral reflectances. The hemispheric-averaged spectral reflectances of the Scanning Imaging Absorption Spectrometer for Atmospheric Cartography (SCIAMACHY) [*Bovensmann et al*., 1999] on the European Space Agency's Environmental Satellite are shown in Figure 13 for data averaged over the period 2003–2010. The reflected shortwave spectral radiances measured over the spectral range 214–1773 nm are shown with the spectral resolution degraded from the raw resolution [*Gottwald et al*., 2011a] to 15 nm. Reflectances measured at longer wavelengths (between 1934–2044 nm and 2259–2386 nm) were not included due to detector problems [*Gottwald et al*., 2011b]. The SH is slightly more reflective than the NH at wavelengths less than about 700 nm which is consistent with a proportionally greater reflectance from clouds in the SH. Conversely, the NH reflectance is larger than the SH reflectance at longer wavelengths which is similarly consistent with a proportionally greater reflectance from land surfaces in the NH.
2. *Interannual variability*. Perhaps, a more subtle example of how the albedo is constrained is evident in the interannual variability of the reflected flux. This variability is dominated by the variability of atmospheric scattering that is primarily a result of cloud variability according to the data summarized in Table 2 and further revealed in Figure 14. Figure 14a presents the zonal and annual average of the $1° \times 1°$ standard

©2015. American Geophysical Union. All Rights Reserved.

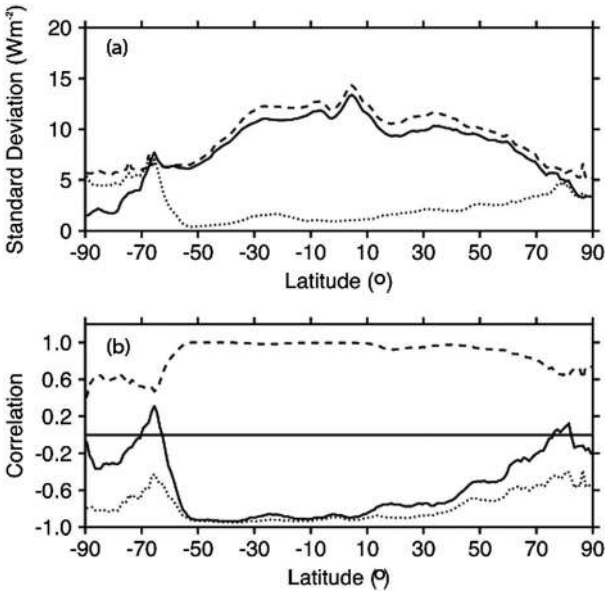

Figure 14. (a) The zonal average of the interannual variability of the reflected flux and the atmospheric and surface contributions to this flux. This variability is defined according to (6a) and (6b) applied to 1° × 1° data. (b). The correlations between TOA flux and the surface flux contribution (solid) and atmospheric contribution (dashed). The dotted line is a similar correlation between the anomalies in the atmospheric and surface contributions.

deviations defined according to (8). The zonal average of the TOA flux deviations is shown together with the atmospheric and surface contributions. Figure 14b is the correlation between the monthly TOA flux anomalies calculated from the 13 year averaged monthly fluxes and the anomalies in surface and atmospheric flux contributions and the correlation between the anomalies in the atmospheric and surface contributions. The negative correlation between the atmospheric and surface contributions shown in Figure 14b is expected, given the negative correlation between atmospheric reflection and atmospheric transmission. Taken together, the results indicate that the interannual anomalies in TOA flux are primarily set by the variability in atmospheric scattering except for the notable regions poleward of 70°N and 70°S. The atmospheric variability also exceeds the TOA variability at all latitudes, and at higher latitudes in particular the TOA flux is much less variable than either of the individual components that produces it (also Table 2). This suggests that there are compensating effects between changes that occur between the surface and within the atmosphere.

7.3. Is There a Simple Explanation for the Observed Hemispheric Symmetry in Albedo?

Whether the symmetry referred to above and the regulation of Earth's albedo relevant to it is a fundamental property of the Earth's climate system is not yet known. Further insight on this symmetry follows from the simple consideration of the planet divided into two zonally averaged boxes. In a steady state, each box neither gains nor loses energy, so the net energy flux of radiation N_i into the top of the ith box ($i = 1,2$) must balance the divergence of energy X_i associated heat transported through the sides of the box by the atmosphere and oceans. Thus,

$$N_i + X_i = 0 \tag{9}$$

where

$$N_i = S_i(1 - R_i) - L_i \tag{10}$$

and $S_i(1 - R_i)$ is the net shortwave (solar) radiation entering at the top of the atmosphere and L_i is the OLR. For the planet in steady state

$$\sum_i N_i = 0 \tag{11}$$

and because the flux of energy carried by the fluid across the boundaries of one box is gained by its neighbors,

$$\sum_i X_i = 0 \tag{12}$$

as required by (9). For the special case of $X_1 = X_2 = 0$, it then follows that L1 = L2 and $S_1(1 - R_1) = S_2(1 - R_2)$ and since $S_1 = S_2$, it follows that $R_1 = R_2$. That is a symmetric energy balance implies a zero cross equatorial heat transport.

The OLR of each hemisphere can be characterized by an effective emission temperature, T_1 and T_2. Since the NH is slightly warmer that the SH [*Kang and Seager*, 2012], it is reasonable also to suppose that the

©2015. American Geophysical Union. All Rights Reserved.

emission temperatures might also differ between the hemispheres given the different surface albedos, temperatures, cloud covers, and cloud properties of the hemispheres. In reality, the hemispheric all-sky OLR difference is smaller than the clear-sky OLR differences due to offsetting effects of clouds. According to the 13 year average of EBAF 2.7r data (Table 3), the 13 year averaged NH all-sky OLR is 240.4 W m^{-2} and 239.2 W m^{-2} for the SH. This slight hemispheric difference in OLR is half the clear-sky OLR differences and is the principal source of the 0.6 W m^{-2} global mean imbalance in the TOA net flux [*Loeb et al*., 2012] occurring in the SH oceans, mostly equatorward of the zero net flux line (36.9°S, Figure 9b). As a result of this slight imbalance, a small amount of heat is transported across the equator from the SH to the NH. According to CERES, the inferred net transport of heat across the equator is 0.2 PW [e.g., *Marshall et al*., 2013]. This net transport is a result of compensating atmospheric heat transported to SH offset by a NH cross equatorial transport to the NH by oceans and appears to be an important diagnostic property of the Earth's climate system. Based on analysis of slab-ocean model experiments, *Frierson and Hwang* [2012] find a direct correlation between the position of the modeled ITCZ and the cross equatorial transport of heat transport, and both *Frierson et al*. [2013] and *Marshall et al*. [2013] argue that the climatological position of the ITCZ is controlled by the oceanic transport of heat across the equator.

8. Summary

The solar energy reflected from Earth is a fundamental component of the Earth's energy balance, and processes that define the albedo of Earth are of elementary relevance to the Earth's climate. This study reviews our understanding of the Earth's albedo as it has progressed to the present time and provides a global perspective of our understanding of the processes that shape it. Based on current-day satellite observations of reflected sunlight, we conclude that

1. Estimates of the albedo of Earth have evolved over time but converged over the past 40 years of satellite record to the present-day value of 0.29 (or equivalently 99.7 W m^{-2} reflected energy). The satellite observations obtained over this period indicate that the albedo of Earth is highly constrained, restricting the degree to which the albedo varies over space and limits the variability of albedo over time.
2. The interannual variability of global reflected flux is 0.2 W m^{-2} which is only 1.4% of the annual cycle of this flux and 0.2% of the total global mean reflected flux [e.g., *Kato*, 2009]. This interannual variability systematically increases from the tropics to the midlatitudes to the polar regions. The major source of albedo variability and the principal mode of regulation are associated with the interannual variations of cloudiness. The small variability observed suggests a high degree of buffering by the albedo of clouds.

We also show, as others before, how the amount of solar energy reflected from each hemisphere is essentially identical. This symmetry appears in broadband data but not in spectral radiances, thus hinting at the importance of such spectral data as a diagnostic tool for studying Earth's climate system. Again, the cloudiness of the planet is the principal regulatory agent that maintains this symmetry with the increased energy reflected from SH clouds precisely balancing the larger reflections from NH land masses. Simple arguments suggest that a symmetric energy balance implies zero cross equatorial transport of heat, which is a condition of a steady state. Although Earth is very near this symmetric state, it is currently out of energy balance with less OLR emitted from the SH than the NH giving rise to the approximate 0.6 W m^{-2} global imbalance observed.

It is also shown how the ability of present-day models of climate in simulating the statistical properties of the energy reflected from Earth varies depending upon the metric used. Models fail to reproduce the observed annual cycle in all components of the albedo with any realism, although they broadly capture the correct proportions of surface and atmospheric contributions to the TOA albedo. A high model bias of albedo has also persisted since the time of CMIP3, mostly during the boreal summer season. Perhaps more importantly, models fail to produce the same degree of interannual constraint on the albedo variability nor do they reproduce the same degree of hemispheric symmetry. The significance of these shortcomings is not yet fully known, but model studies of hypothetical slab-ocean worlds suggest that interhemispheric changes in albedo can grossly affect the climate states of those worlds, shifting the ITCZ [*Voigt et al*., 2013, 2014; *Frierson and Hwang*, 2012] and altering the amount of heat moved poleward [e.g., *Enterton and Marshall*, 2010].

©2015. American Geophysical Union. All Rights Reserved.

Acknowledgments

We would like to acknowledge Yolanda Roberts, NASA LaRC, for processing SCIAMACHY data, Claudia Stubenrauch for confirming the same hemispheric cloud differences shown in Figure 3 in the GEWEX cloud assessment data archive, and Norm Loeb for comments on the use on CERES EBAF data. All data described in this paper are available through relevant data repositories. The CMIP data are available from http://cmip-pcmdi.llnl.gov/cmip5/ and CERES are available at http://ceres.larc.nasa.gov/products.php?product=EBAF-TOA. The SCIAMACHY data are available from one of the authors (P.P.) on request. The CloudSat CALIPSO data used to produce Figure 3 are available from the CloudSat data processing data center http://www.cloudsat.cira.colostate.edu.

The Editor for this paper was Alan Robock. He would like to thank Norman Loeb and two anonymous reviewers for their review assistance on this manuscript.

References

Abbot, C. G., and F. E. Fowle (1908), Radiation and terrestrial temperature, in *Annals of the Astrophysical Observatory of the Smithsonian Institution*, vol. 2, pp. 125–224, Smithsonian, Wash.

Aldrich, L. B. (1922), The reflecting power of clouds, in *Annals of the Astrophysical Observatory of the Smithsonian Institution*, vol. 4, appendix III, pp. 375–381.

Allan, R. P., A. Slingo, and M. A. Ringer (2002), Influence of dynamics on the changes in tropical cloud radiative forcing during the 1998 El Niño, *J. Clim.*, *15*, 1979–1986.

Andrews, T., J. M. Gregory, M. J. Webb, and K. E. Taylor (2012), Forcing, feedbacks and climate sensitivity in CMIP5 coupled atmosphere-ocean climate models, *Geophys. Res. Lett.*, *39*, L09712, doi:10.1029/2012GL051607.

Barkstrom, B. R. (1984), The Earth Radiation Budget Experiment (ERBE), *Bull. Am. Meteorol. Soc.*, *65*(11), 1170–1185.

Bauer, F., and H. Phillips (1934), Der Warmehaushalt der Lufthull der Nordhalbkugeilm Januar und Juli und zur Zeit der quinoktien und Solstitien, *Gerlands Beitr. Geophys.*, *41*, 160–207.

Baur, F., and H. Phillips (1935), Der Warmehaushalt der Lufthfille der Nordhalbkugeilm Januaru nd Juli und zur Zeit der •quinoktien und Solstitien, *Gerlands Beitr. Geophys.*, *45*, 82–132.

Bender, F., H. Rodhe, R. J. Charlson, A. M. L. Ekman, and N. Loeb (2006), 22 views of the global albedo—Comparison between 20 GCMs and two satellites, *Tellus*, *58A*, 320–330.

Bony, S., and J.-L. Dufresne (2005), Marine boundary layer clouds at the heart of tropical cloud feedback uncertainties in climate models, *Geophys. Res. Lett.*, *32*, L20806, doi:10.1029/2005GL023851.

Bovensmann, H., J. P. Burrows, M. Buchwitz, J. Frerick, S. Noël, V. V. Rozanov, K. V. Chance, and A. P. H. Goede (1999), SCIAMACHY: Mission objectives and measurement modes, *J. Atmos. Sci.*, *56*(2), 127–150.

Brooks, C. E. P. (1930), The mean cloudiness over the Earth, *Mem. R. Meteorol. Soc.*, *1*, 127–138.

Budyko, M. I. (1969), The effect of solar radiation variations on the climate of the Earth, *Tellus*, *21*, 611–619.

Cahalan, R. F., and G. R. North (1979), A stability theorem for energy-balance climate models, *J. Atmos. Sci.*, *36*, 1,205–1,216.

Caldwell, P. M., C. S. Bretherton, M. D. Zelinka, S. A. Klein, B. D. Santer, and B. M. Sanderson (2014), Statistical significance of climate sensitivity predictors obtained by data mining, *Geophys. Res. Lett.*, *41*, 1803–1808, doi:10.1002/2014GL059205.

Cess, R. D., M. Zhang, P. H. Wang, and B. A. Wielicki (2001), Cloud structure anomalies over the tropical Pacific during the 1997/98 El Niño, *Geophys. Res. Lett.*, *28*, 4547–4550.

Chen Y.-C., M. W. Christensen, L. Xue, A. Sorooshian, G. L. Stephens, R. M. Rasmussen, and J. H. Seinfeld (2012), Occurrence of lower cloud albedo in ship tracks, *Atmos. Chem. Phys.*, *12*, 8223–8235, doi:10.5194/acp-12-8223-2012.

Christensen, M. W., and G. L. Stephens (2011), Microphysical and macrophysical responses of marine srtratocumulus polluted by underlying ships: Evidence of cloud deepening, *J. Geophys. Res.*, *116*, D03201, doi:10.1029/2010JD014638.

Clement, A., R. Burgman, and J. Norris (2009), Observational and model evidence for positive low-level cloud feedback, *Science*, *325*(5939), 460–464, doi:10.1126/science.1171255.

Danjon, A. (1928), Recherchess ur la photom6trie de la lumiere cendree et l'albedo de la terre, *Ann. Obs. Strasbourg*, *2*, 165–180.

Danjon, A. (1936), Nouvelles recherches sur la photom6trie de la lumiere cendree et l'albedo de la terre, *Ann. Obs. Strasbourg*, *3*, 139–180.

Dines, W. H. (1917), The heat balance of the atmosphere, *Q. J. R. Meteorol. Soc.*, *43*(12), 151–158.

Doelling, D. R., N. Loeb, D. F. Keyes, M. L. Nordeen, D. Morstad, B. A. Wielicki, D. F. Young, and M. Sun (2013), Geostationary enhanced temporal interpolation for CERES flux products, *J. Atmos. Oceanic Technol.*, doi:10.1175/JTECH-D-12-00136.1.

Donohoe, A., and D. Battisti (2012), What determines meridional heat transport in climate models?, *J. Clim.*, *25*, 3832–3850.

Enterton, D., and J. M. Marshall (2010), Explorations of atmosphere-ocean-ice climates on an aquaplanet and their meridional energy transports, *J. Atmos. Sci.*, *66*, 1593–1611.

Flatau, P. J., and G. L. Stephens (1988), On the fundamental solution of the radiative transfer equation, *J. Geophys. Res.*, *93*(D9), 11,037–11,050, doi:10.1029/JD093iD09p11037.

Frierson, D. M. W., and Y. T. Hwang (2012), Extra-tropical influence on ITCZ shifts in slab ocean simulations of global warming, *J. Clim.*, *25*, 720–733.

Frierson, D. M. W., N. Fuckar, R. Seager, S. M. Kang, A. Donohue, E. A. Maroon, X. Liu, and D. Battisti (2013), Contribution of ocean overturning circulation to tropical rainfall peak in the Northern Hemisphere, *Nat. Geosci.*, *6*, 940–944.

Fritz, S. (1948), The albedo of the ground and atmosphere, *Bull. Am. Meteorol. Soc.*, *29*, 303–312.

Fritz, S. (1950), Measurement of the albedo of clouds, *Bull. Am. Meteorol. Soc.*, *31*, 25–27.

Gottwald, M., R. Hoogeveen, C. Chlebek, H. Bovensmann, J. Carpay, G. Lichtenberg, E. Krieg, P. Lutzow-Wentzky, and T. Watts (2011a), *SCIAMACHY—Exploring the Earth's Changing Atmosphere*, chap. 3, pp. 29–46, Springer, New York.

Gottwald, M., R. Hoogeveen, C. Chlebek, H. Bovensmann, J. Carpay, G. Lichtenberg, E. Krieg, P. Lutzow-Wentzky, and T. Watts (2011b), *SCIAMACHY—Exploring the Earth's Changing Atmosphere*, chap. 6, pp. 77–97, Springer, New York.

Gray, L. J., et al. (2010), Solar Influences on Climate, *Rev. Geophys.*, *48*, RG4001, doi:10.1029/2009RG000282.

Haeffelin, M., R. Kandel, and C. Stubenrauch (1999), Improved diurnal interpolation of reflected broadband shortwave observations using ISCCP data, *J. Atmos. Oceanic Technol.*, *16*, 38–54.

Haigh J. D. (1996), The impact of solar variability on climate, *Science*, *272*, 981–984.

Hall, A., and X. Qu (2006), Using the current seasonal cycle to constrain snow albedo feedback in future climate change, *Geophys. Res. Lett.*, *33*, L03502, doi:10.1029/2005GL025127.

Hartmann, D., K. J. Kowalewsky, and M. Michelsen (1991), Diurnal variation of outgoing longwave radiation and albedo from ERBE scanner data, *J. Clim.*, *4*, 598–617.

Herschel, W. (1801), Observations tending to investigate the nature of the Sun in order to find the causes or symptoms of its variable emission of light and heat: With remarks on the use that may possibly be drawn from solar observations, *Philos Trans. R. Soc. London*, doi:10.1098/rstl.1801.0015.

Houghton, H. G. (1954), On the annual heat balance of the Northern Hemisphere, *J. Meteorol.*, *11*, 1–9.

House, F. B., A. Gruber, G. E. Hunt, and A. T. Mecherikunnel (1986), History of satellite mission and measurements of the Earth radiation budget (1957–1984), *Rev. Geophys.*, *24*, 357–377, doi:10.1029/RG024i002p00357.

Hunt, G. E., R. Kandel, and A. T. Mecherikunnel (1986), A history of presatellite investigation of the Earth's radiation budget, *Rev. Geophys.*, *24*(2), 351–356, doi:10.1029/RG024i002p00351.

Intergovernmental Panel on Climate Change (2001), Climate change 2001: The scientific basis, in *Contribution of Working Group I to the Third Assessment Report of the Intergovernmental Panel on Climate Change*, edited by J. T. Houghton et al., 881 pp., Cambridge Univ. Press, Cambridge, U. K., and New York.

©2015. American Geophysical Union. All Rights Reserved.

Jacobowitz, H. R., J. Tighe, and Nimbus 7 ERB Experiment Team (1984), The Earth radiation budget derived from Nimbus 7 ERB Experiment, *J. Geophys. Res.*, *89*, 5021–5038, doi:10.1029/JD089iD04p05021.
Kandel, R., and M. Viollier (2005), Planetary radiation budget, *Space Sci. Rev.*, doi:10.1007/s11214-005-6482-6.
Kandel, R., and M. Viollier (2010), Observation of the Earth's radiation budget from space, *C. R. Geosci.*, *342*, 286–300, doi:10.1016/j.crte.2010.01.005.
Kang, S. M., and R. Seager (2012), Croll revisited: Why is the Northern Hemisphere warmer than the Southern Hemisphere?. [Available at http://academinccommons.columbia.edu/catalog/ac:153364.]
Kato, S. (2009), Interannual variability of global radiation budget, *J. Clim.*, *22*, 4893–4907.
Kato, S., and N. G. Loeb (2005), Top-of-atmosphere shortwave broadband observed radiance and estimated irradiance over polar regions from clouds and the Earth's Radiant Energy System (CERES) instruments on Terra, *J. Geophys. Res.*, *110*, D07202, doi:10.1029/2004JD005308.
Kato, S., et al. (2011), Improvements of top-of-atmosphere and surface irradiance computations with CALIPSO-, CloudSat-, and MODIS-derived cloud and aerosol properties, *J. Geophys. Res.*, *116*, D19209, doi:10.1029/2011JD016050.
Kato, S., N. G. Loeb, F. G. Rose, D. R. Doelling, D. A. Rutan, T. E. Caldwell, Y. Lisan, and R. A. Weller (2013), Surface irradiances consistent with CERES-derived top-of-atmosphere shortwave and longwave irradiances, *J. Clim.*, *26*(9), 2719–2740.
Koppen, W. (1873), Uber mehrjahrige Perioden der Witterung insbesondere uber die 11 jahrige Periode der Temperatur, *Z. Oesterr. Ges. Meteorol.*, *8*, 241.
Labitzke, K., and H. van Loon (1992), Association between the 11-year Cycle and the atmosphere V: Atmosphere, *J. Clim.*, *5*, 240–251.
Latham, J. (2002), Amelioration of global warming by controlled enhancement of albedo and longevity of low-marine clouds, *Atmos. Sci. Lett.*, *3*, 52, doi:10.1006/asle.2002.0048.
Loeb, G. N., B. A. Wielicki, D. R. Doelling, G. L. Smith, D. F. Keyes, S. Kato, N. Manalo-Smith, and T. Wong (2009), Toward optimal closure of the Earth's top-of-atmosphere radiation budget, *J. Clim.*, *22*, 748–766, doi:10.1175/2008JCLI2637.1.
Loeb, N., and N. Manalo-Smith (2005), Top-of-atmosphere Direct Radiative Effect of Aerosol over Global Oceans from Merged CERES and MODIS observations, *J. Clim.*, *18*, 3506–3526.
Loeb, N., et al. (2012), Heating of Earth's climate system continues despite lack of surface warming in past decade, *Nat. Geosci.*, *5*, 110–113, doi:10.1038/ngeo1375.
Loeb, N. G., N. Manalo-Smith, S. Kato, W. F. Miller, S. K. Gupta, P. Minnis, and B. A. Wielicki (2003), Angular distribution models for top-of-atmosphere radiative flux estimation from the Clouds and the Earth's Radiant Energy System instrument on the Tropical Rainfall Measuring Mission satellite. Part I: Methodology, *J. Appl. Meteorol.*, *42*, 240–265.
Loeb, N. G., S. Kato, K. Loukachine, and M. N. Natividad (2005), Angular distribution models for top-of-atmosphere radiative flux estimation from the Clouds and the Earth's Radiant Energy System instrument on the Terra Satellite. Part I: Methodology, *J. Appl. Meteorol.*, *22*, 338–351.
Loeb, N. G., B. A. Wielicki, F. G. Rose, and D. R. Doelling (2007), Variability in global top-of-atmosphere shortwave radiation between 2000 and 2005, *Geophys. Res. Lett.*, *34*, L03704, doi:10.1029/2006GL028196.
London, J. A. (1957), A study of the atmospheric heat balance, Final report, contract USAF8S1911221165, New York Univ., New York.
Lovelock, J. E. (1967), Gaia as seen through the atmosphere, *Atmos. Environ.*, *6*(8), 579–580.
Mace, G. G., Q. Zhang, M. Vaughn, R. Marchand, G. Stephens, C. Trepte, and D. Winker (2009), A description of hydrometeor layer occurrence statistics derived from the first year of merged CloudSat and CALIPSO data, *J. Geophys. Res.*, *114*, D00A26, doi:10.1029/2007JD009775.
Marshall, J., A. Donohue, D. Ferreira, and D. McGee (2013), The ocean's role in setting the mean position of the Inter-Tropical Convergence Zone, *Clim. Dyn.*, doi:10.1007/s00382-013-1767-z.
Moberg, A., D. M. Sonechkin, K. Holmgren, N. M. Datsenko, and W. Karlen (2005), Highly variable Northern Hemisphere temperatures reconstructed from low- and high-resolution proxy data, *Nature*, *433*, 613–617.
Myre, G., et al. (2013), Anthropogenic and natural radiative forcing, Chap 8 Intergovernmental Panel on Climate Change, 5th Assessment.
North, G. R., R. F. Cahalan, and J. A. Coakley (1981), Energy balance climate models, *Rev. Geophys. Space Phys.*, *19*, 91–121.
Pallé, E., P. R. Goode, P. Montañés-Rodriguez, and S. E. Koonin (2004), Changes in the Earth's reflectance over the past two decades, *Science*, *304*, 1299–1301.
Paltridge, G. W. (1980), Cloud Radiation feedback to climate, *Q. J. R. Meteorol. Soc.*, *106*, 895–899.
Randel, D. L., and T. H. VonderHaar (1990), On the interannual variation of the Earth radiation budget, *J. Clim.*, *3*, 1168–1173.
Ringer, M. A. (1997), Interannual variability of the Earth's radiation budget: Some regional studies, *Int. J. Clim.*, *17*, 929–951.
Ringer, M. A., and K. P. Shine (1997), Sensitivity of the Earth's radiation budget to interannual variations in cloud amount, *Clim. Dyn.*, *13*, 213–222.
Robinson, G. D. (1956), The use of surface observations to estimate the local energy balance of the atmosphere, *Proc. R. Soc. London. Set. A*, *236*, 160–171.
Robinson, G. D. (1958), Some observations from aircraft of surface albedo and the albedo and absorption of cloud, *Arch. Meteorol. Geophys. Bioklimatol., Ser. B*, *9*(H.1), 28–41.
Russell, H. N. (1916), On the albedo of the planets and their satellites, *Astrophys. J.*, *43*, 173–196.
Simpson, G. C. (1928a), Some studies in terrestrial radiation, *Mem. R. Meteorol. Soc.*, *2*(16), 69–95.
Simpson, G. C. (1928b), Further studies in terrestrial radiation, *Mem. R. Meteorol. Soc.*, *3*(21), 1–26.
Simpson, G. C. (1929), The distribution of terrestrial radiation, *Mem. R. Meteorol. Soc.*, *3*(23), 36–41.
Smith, E. A., and M. R. Smith (1987), Interannual variability of the tropical radiation balance and the role of extended cloud system, *J. Atmos. Sci.*, *44*, 3210–3234.
Smith, G. L., D. Rutan, T. P. Charlock, and D. Bess (1990), Annual and interannual variations of absorbed solar radiation based on a 10-year data set, *J. Geophys. Res.*, *95*(D10), 16,639–16,652, doi:10.1029/JD095iD10p16639.
Soden, B. J., I. M. Held, R. Colman, K. M. Shell, J. T. Kiehl, and C. A. Shields (2008), Quantifying climate feedbacks using radiative kernels, *J. Clim.*, *21*(14), 3504–3520.
Sofia, S., and L. H. Li (2001), 2001 solar variability and climate, *J. Geophys. Res.*, *106*, 12,969, doi:10.1029/2000JA000379.
Sommerville, R., and L. A. Remer (1984), Cloud optical thickness feedbacks in the CO_2 climate problem, *J. Geophys. Res.*, *89*, 9668–9672, doi:10.1029/JD089iD06p09668.
Stephens, G. L. (2005), Cloud feedbacks in the climate system: A critical review, *J. Clim.*, *18*, 237–273.
Stephens, G. L., and T. J. Greenwald (1991), The Earth's radiation budget and its relation to atmospheric hydrology 2. Observations of cloud effects, *J. Geophys. Res.*, *96*(D8), 15,325–15,340, doi:10.1029/91JD00972.
Stephens, G. L., and C. Kummerow (2007), The remote sensing of clouds and precipitation from space: A review, *J. Atmos. Sci.*, *64*, 3742–3765.
Stephens, G. L., and S. C. Tsay (1990), On the cloud absorption anomaly, *Q. J. R. Meteorol. Soc.*, *116*, 671–704.

©2015. American Geophysical Union. All Rights Reserved.

Stephens, G. L., G. G. Campbell, and T. H. V. Haar (1981), Earth radiation budgets, *J. Geophys. Res.*, *86*(C10), 9739–9760, doi:10.1029/JC086iC10p09739.
Stephens, G. L., et al. (2002), The Cloudsat Mission and the A-Train, *Bull. Am. Meteorol. Soc.*, *83*, 1771–1790.
Stephens, G. L., J. Li, M. Wild, C. A. Clayson, N. Loeb, S. Kato, T. L'Ecuyer, P. W. Stackhouse Jr., and T. Andrews (2012), An update on Earth's energy balance in light of the latest global observations, *Nat. Geosci.*, *5*, 691–696.
Stevens, B., and G. Feingold (2009), Untangling aerosol effects on clouds and precipitation in a buffered system, *Nature*, *7461*(7264), 607–613.
Stevens, B., and S. E. Schwartz (2012), Observing and modeling Earth's energy flows, *Surv. Geophys.*, *33*, doi:10.1007/s10712-012-9184.0.
Stone, P. H. (1978), Constraints on dynamical transports of energy on a spherical planet, *Dyn. Atmos. Oceans*, *2*, 123–139.
Stubenrauch, C. J., et al. (2013), Assessment of global cloud datasets from satellites: Project and database initiated by the GEWEX radiation panel, *Bull. Am. Meteorol. Soc.*, *94*, 1031–1049, doi:10.1175/BAMS-D-12-00117.1.
Taylor, K. E., M. Crucifix, P. Bracconet, C. D. Hewitt, C. Deautriaux, A. J. Broccoli, J. F. B. Mitchell, and M. J. Webb (2007), Estimating shortwave radiative forcing and response in climate models, *J. Clim.*, *20*, 2530–2543.
Taylor, K. E., R. J. Stouffer, and G. A. Meehl (2012), An overview of CMIP5 and the experiment design, *Bull. Am. Meteorol. Soc.*, *93*, 485–498, doi:10.1175/BAMS-D-11-00094.1.
Taylor, P. C. (2014), Variability of monthly diurnal cycle composites of TOA radiative fluxes in tropics, *J. Atmos. Sci.*, *71*, doi:10.1175/JAS-D-13-0112.1.
Taylor, P. C., and N. G. Loeb (2013), Impact of sun-synchronous diurnal sampling on tropical TOA flux interannual variability and trend, *J. Clim.*, *26*, doi:10.1175/JCLI-D-12-00416.1.
Very, F. W. (1912), The Earth's albedo, *Astron. Nachr.*, *196*, 269–290.
Vial, J., J.-L. Dufresne, and S. Bony (2013), On the interpretation of inter-model spread in CMIP5 climate sensitivity estimates, *Clim. Dyn.*, doi:10.1007/s00382-013-1725-9.
Voigt, A., B. Stevens, J. Bader, and T. Mauristen (2013), The observed hemispheric symmetry in reflected shortwave irradiance, *J. Clim.*, *26*, 468–477.
Voigt, A., B. Stevens, J. Bader, and T. Mauritsen (2014), Compensation of hemispheric albedo asymmetries by shifts of the ITCZ and tropical cloud, *J. Clim.*, *27*, 1029–1044.
Vonder Haar, T. H., and V. Suomi (1971), Measurements of the Earth's radiation budget from satellites during a 5 year period. Part I: Extended time and space means, *J. Atmos. Sci.*, *28*, 305–314.
Watson, A. J., and J. E. Lovelock (1983), Biological homeostasis of the global environment: The parable of Daisyworld, *Tellus*, *35B*, 284–289.
Wielicki, B. A., B. R. Barkstrom, E. F. Harrison, R. B. Lee III, G. L. Smith, and J. E. Cooper (1996), Clouds and the Earth's Radiant Energy System (CERES): An Earth observing system, *Bull. Am. Meteorol. Soc.*, *72*, 853–868.
Wielicki, B. A., et al. (1998), Clouds and the Earth's Radiant Energy System (CERES): Algorithm overview, *IEEE Trans. Geosci. Remote Sens.*, *36*(4), 1127–1141.
Wielicki, B. A., et al. (2002), Evidence for large decadal variability in the tropical mean radiative energy budget, *Science*, *295*, 841–844.
Wielicki, B. A., T. Wong, N. G. Loeb, P. Minnis, K. J. Priestley, and R. Kandel (2005), Changes in Earth's albedo measured by satellite, *Science*, *308*, 825.
Wong, T., B. A. Wielicki, R. B. Lee III, G. L. Smith, K. A. Bush, and J. K. Willis (2006), Reexamination of the observed decadal variability of the Earth radiation budget using altitude-corrected ERBE/ERBS Nonscanner WFOV Data, *J. Clim.*, *19*, 4028–4040.

©2015. American Geophysical Union. All Rights Reserved.